https://doi.org/10.1093/plcell/koad231 THE PLANT CELL 2023: 35: 4266–4283

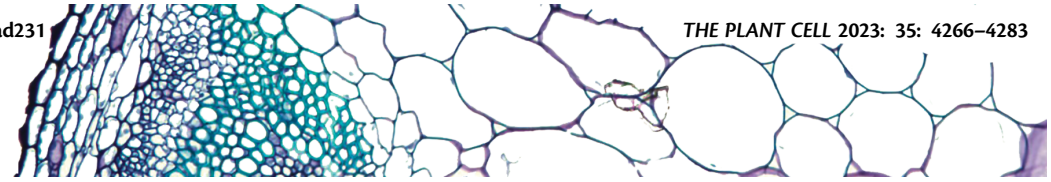

Research Article

Microtubule-associated protein SlMAP70 interacts with IQ67-domain protein SlIQD21a to regulate fruit shape in tomato

Zhiru Bao,[1,2] **Ye Guo**,[1,2] **Yaling Deng**,[1,2] **Jingze Zang**,[1,2] **Junhong Zhang**,[1] **Yingtian Deng**,[1] **Bo Ouyang**,[1] **Xiaolu Qu**,[1] **Katharina Bürstenbinder**[3] **and Pengwei Wang**[1,2,*]

1 National Key Laboratory for Germplasm Innovation and Utilization of Horticultural Crops, College of Horticulture and Forestry Sciences, Huazhong Agricultural University, Wuhan 430070, China
2 Hubei Hongshan Laboratory, Wuhan 430070, China
3 Department of Molecular Signal Processing, Leibniz Institute of Plant Biochemistry, Halle (Saale) 06120, Germany

*Author for correspondence: wangpengwei@mail.hzau.edu.cn
The author responsible for distribution of materials integral to the findings presented in this article in accordance with the policy described in the Instructions for Authors (https://academic.oup.com/plcell/pages/General-Instructions) is: Pengwei Wang (wangpengwei@mail.hzau.edu.cn).

Abstract

Tomato (*Solanum lycopersicum*) fruit shape is related to microtubule organization and the activity of microtubule-associated proteins (MAPs). However, insights into the mechanism of fruit shape formation from a cell biology perspective remain limited. Analysis of the tissue expression profiles of different microtubule regulators revealed that functionally distinct classes of MAPs, including members of the plant-specific MICROTUBULE-ASSOCIATED PROTEIN 70 (MAP70) and IQ67 DOMAIN (IQD, also named SUN in tomato) families, are differentially expressed during fruit development. *SlMAP70-1–3* and *SlIQD21a* are highly expressed during fruit initiation, which relates to the dramatic microtubule pattern rearrangements throughout this developmental stage of tomato fruits. Transgenic tomato lines overexpressing *SlMAP70-1* or *SlIQD21a* produced elongated fruits with reduced cell circularity and microtubule anisotropy, while their loss-of-function mutants showed the opposite phenotype, harboring flatter fruits. Fruits were further elongated in plants coexpressing both *SlMAP70-1* and *SlIQD21a*. We demonstrated that SlMAP70s and SlIQD21a physically interact and that the elongated fruit phenotype is likely due to microtubule stabilization induced by the SlMAP70–SlIQD21a interaction. Together, our results identify SlMAP70 proteins and SlIQD21a as important regulators of fruit elongation and demonstrate that manipulating microtubule function during early fruit development provides an effective approach to alter fruit shape.

Introduction

The genetic basis of tomato (*Solanum lycopersicum*) fruit shape has been associated with several genes that are grouped into different categories. The first category includes genes that regulate fruit locule number such as *FASCIATED* (*FAS*) and *LOCULE NUMBER* (*LC*), which encode a homeodomain transcription factor WUSCHEL (WUS) and a CLE small peptide protein CLAVATA3 (CLV3), respectively (Muños et al. 2011; Chu et al. 2019). The second category includes genes that regulate fruit cell division or elongation such as *OVATE* and *SUN*, which encode a negative regulatory protein OVATE FAMILY PROTEIN 20 (OFP20) and a calmodulin-binding protein SUN1, respectively (Liu et al. 2002; Xiao et al. 2008).

Changes in cell division and expansion during early fruit development are believed to have direct impacts on fruit yield and quality. In tomato, OFPs regulate cell division patterns during fruit development by interacting with TONNEAU1 RECRUITING MOTIF proteins (TRMs), which are essential for the recruitment of the TON1-TRM-PP2A (TTP) complex to microtubules and the assembly of the

Received April 19, 2023. Accepted August 06, 2023. Advance access publication September 5, 2023

IN A NUTSHELL

Background: Genes encoding microtubule-binding proteins have emerged as conserved trait loci for fruit shape regulation with important roles during domestication. While microtubule-binding proteins have been reported in many fruit crops, most studies were performed using forward genetics or population genetics approaches. Thus, in-depth molecular and cell biology insight is lacking.

Question: How are cortical microtubules organized in fruit tissue? From a cell biology perspective, which proteins regulate microtubule dynamics and organization in tomato fruits?

Findings: We identified the microtubule-associated proteins SlMAP70s and SlIQD21a as important regulators of tomato fruit shape. These proteins interact and affect microtubule stability, which may contribute to the rearrangement of cortical microtubules and cell growth patterns underlying organ shape. Transgenic tomato lines overexpressing *SlMAP70-1* produced elongated fruits with reduced cell circularity and microtubule anisotropy, while loss-of-function mutants exhibited flatter fruits. Fruits were further elongated in plants coexpressing both *SlMAP70-1* and *SlIQD21a*.

Next steps: These findings shed light on the functional regulation of microtubule organization and provide a powerful approach for future studies on fruit shape regulation in fruit crops.

preprophase band (PPB) during cell division (Spinner et al. 2013; Schaefer et al. 2017; Wu et al. 2018). On the other hand, SUN1 protein, also known as SlIQD12, localizes to microtubules and likely regulates cell number and fruit shape by altering microtubule structure during the cell division process (Xiao et al. 2008; Huang et al. 2013; Bürstenbinder et al. 2017; Bao et al. 2021).

The cellular functions of SUN/IQD proteins are likely conserved in different plant species. Overexpression or knockout of *AtIQDs* in *Arabidopsis* (*Arabidopsis thaliana*) correlates with altered growth and reorganized cortical microtubule (CMT) arrays (Bürstenbinder et al. 2017; Mitra et al. 2019; Kumari et al. 2021; Zang et al. 2021). Such phenomenon is also found in grain/fruit morphogenesis of rice (*Oryza sativa*) (Duan et al. 2017; Liu et al. 2017; Yang et al. 2020), cucumber (*Cucumis sativus*), and watermelon (*Citrullus lanatus*) species (Pan et al. 2017, 2020; Dou et al. 2018). Collectively, these findings imply that modulating *SUN/IQD* gene expression and activity changes organ shape and that different SUN/IQD members may be functionally redundant in this process.

At the molecular level, SUN/IQD proteins are proposed to function as scaffolding proteins in cell signaling (Abel et al. 2013; Bürstenbinder et al. 2013). *Arabidopsis* IQD proteins have been reported to interact with various microtubule-associated proteins (MAPs), including the microtubule-severing enzyme KATANIN1 (KTN1) (Li et al. 2021), KINESIN LIGHT CHAIN-RELATED (KLCR) proteins (Liu et al. 2016; Zang et al. 2021), PHRAGMOPLAST ORIENTING KINESINs (POKs), and PLECKSTRIN HOMOLOGY GTPASE ACTIVATING PROTEINs (PHGAPs) (Kumari et al. 2021) to regulate apical hook formation, cellulose deposition, cell morphogenesis, and cell division-plane orientation and establishment, respectively. These observations support the idea that distinct classes of MAPs regulate cell anisotropic growth, division patterns, and overall organ shape via differential microtubule-modulating activities. These activities likely are fine-tuned by differential and dynamic interactions between functionally distinct IQDs and MAPs. However, MAPs are essential during tomato fruit morphogenesis, and whether similar mechanisms are found in fruit morphogenesis remains to be confirmed.

MICROTUBULE-ASSOCIATED PROTEIN 70 (MAP70) proteins belong to a family of plant-specific MAPs (Korolev et al. 2005, 2007) and are divided into two major clades, the MAP70-1 and MAP70-5 clades (Fig. 1A; Pesquet et al. 2011). In *Arabidopsis*, MAP70-5 regulates CMT organization within the inner side of endodermal cells via its bundling effect, changing the endodermal cell wall to facilitate lateral root morphogenesis (Stöckle et al. 2022). However, MAP70-1 and MAP70-5 isoforms only share a maximum similarity of 37% in protein sequence (Pesquet et al. 2011), suggesting that MAP70-1 may have different functions from MAP70-5.

Here, we show that *MAP70-1* from tomato is highly expressed at the early fruit developmental stages and identify MAP70 proteins as important regulators of CMT array patterning and fruit morphogenesis in tomato. Knock-out mutants of *SlMAP70-1* and *SlMAP70-2* display flat fruits while overexpressing *SlMAP70-1* induces the opposite effect with plants producing longer fruits. The altered fruit shape is mainly due to changes in cell shape and CMT arrays starting from ovary development. A yeast 2-hybrid (Y2H) test identified SlIQD21a as an interactor of SlMAP70 proteins. In the presence of SlMAP70-1 and SlIQD21a, the average microtubule length increases significantly and tends to form whorl-like arrays in *Nicotiana benthamiana* leaf epidermal cells. Overexpression of *SlIQD21a* or *SlMAP70-1* induces the production of elongated fruits, and this phenotype is further enhanced upon coexpression of *SlIQD21a* and *SlMAP70-1*. These results identify SlMAP70s as important regulators of fruit shape that function together with SlIQD21a, providing mechanistic insights and in-depth subcellular observations of microtubule organization underlying fruit shape regulation in tomato.

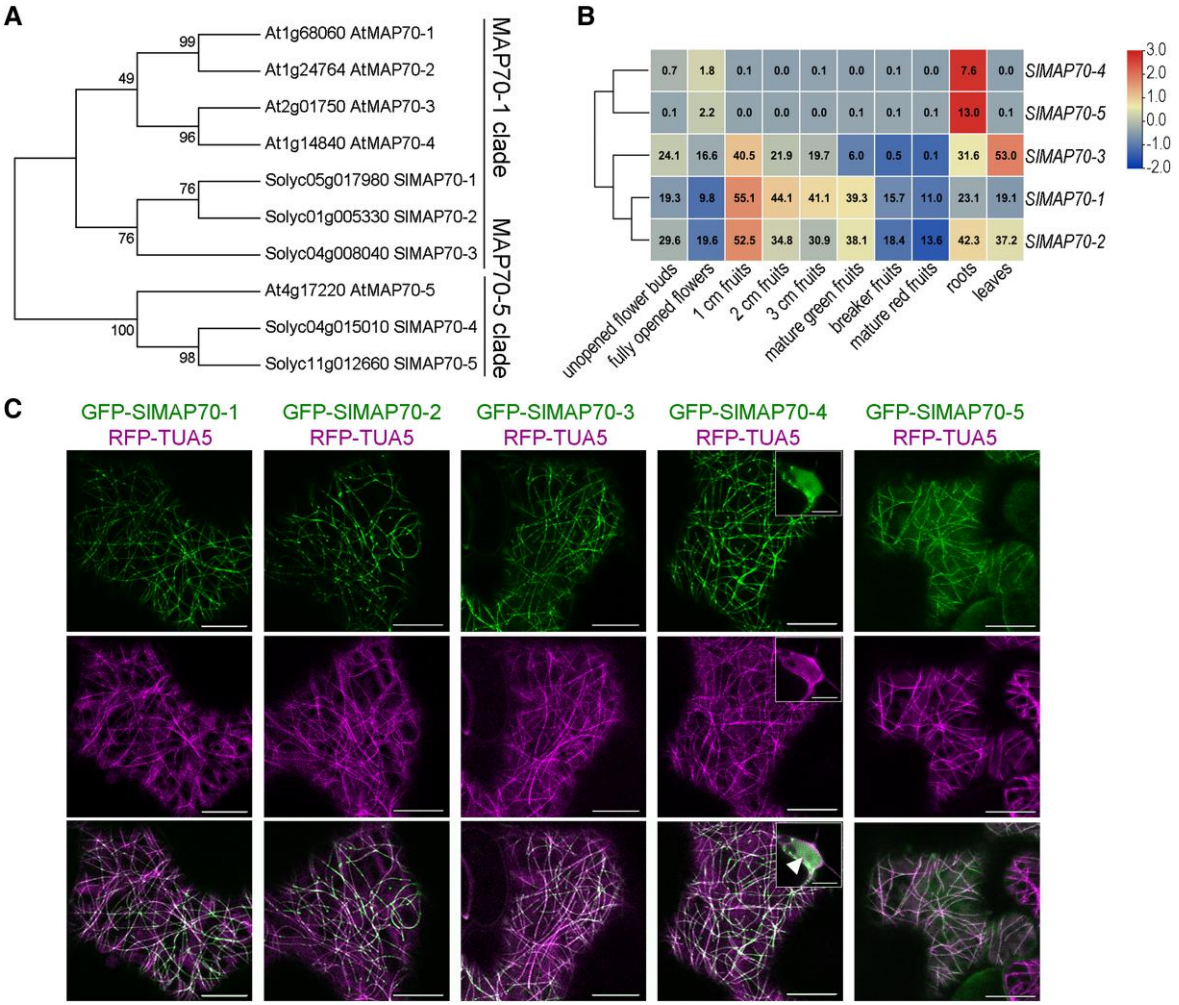

Figure 1. The expression pattern and localization analysis of tomato MAP70 proteins. **A)** Phylogenetic tree of tomato and *Arabidopsis* MAP70 protein sequences, numbers at the tree forks indicated bootstrap values. **B)** Hierarchical clustering of expression values of *SlMAP70* genes in different tissues of tomato cultivar 'Heinz'. Red color indicates a high expression. Blue indicates a low expression. The RNA-seq data were downloaded from the tomato functional genomics database (Tomato Genome Consortium 2012, http://ted.bti.cornell.edu/). **C)** Subcellular localization of SlMAP70 proteins in *N. benthamiana* leaf epidermal cells. Arrowhead indicated the nucleus structure. Bars: 10 μm.

Results

SlMAP70-1 is highly expressed at the early stage of tomato fruit development

Microtubule activity is essential for cell morphogenesis and organ shape formation (Eng and Sampathkumar 2018; Buschmann and Müller 2019). To identify microtubule-related candidates involved in tomato fruit size regulation or shape formation, we analyzed the expression of multiple *MAP* genes in tomato reproductive organs during fruit development. We found that several members of *SPIRAL1* (*SPR1*), *SPIRAL2* (*SPR2*), *TONNEAU2* (*TON2*), *WAVE-DAMPENED2* (*WVD2*), and *MAP70* homologs are highly expressed (Supplemental Fig. S1) during this stage, suggesting these genes may be involved in fruit development. *SlMAP70* genes were chosen for further characterization, as their homologs also exhibit a very high level of expression in fruits of other species (e.g. cucumber; Jiang et al. 2015). BLAST search identified 5 homologs of *MAP70* genes in the tomato genome (version SL4.0, https://solgenomics.net/). Phylogenetic and expression analysis indicated that SlMAP70-1, SlMAP70-2, and SlMAP70-3 proteins belong to the MAP70-1 clade, which is highly expressed in fruits, whereas SlMAP70-4 and SlMAP70-5 proteins belong to the MAP70-5 clade that is specifically expressed in roots (Fig. 1, A and B).

We cloned all 5 members of the *SlMAP70* gene family, generated green fluorescence protein (GFP) fusion constructs, and analyzed their subcellular localization using *N. benthamiana* transient expression assays. In leaf epidermal cells, all GFP-SlMAP70 proteins localized to CMTs that were labeled with red fluorescence protein (RFP)-Tubulin5α (RFP-TUA5); interestingly, some SlMAP70 signals were also enriched at specific foci distributed along the filaments (Fig. 1C). During cell division, which was induced by the ectopic expression of *cyclin D3;1* (*CYCD3:1*) (Xu et al. 2020),

most GFP-SlMAP70 proteins colocalized with microtubules at the spindle and phragmoplast, except for GFP-SlMAP70-4, which also labels the cell plate in telophase and the nucleus in interphase (Fig. 1C; Supplemental Fig. S2). As most *SlMAP70* genes share high sequence similarity, *SlMAP70-1*, which has the strongest expression at the fruit initiation stage (Fig. 1B), was selected for further functional studies.

Tomato fruit elongation and cell morphogenesis are controlled by SlMAP70 activity

Tomato (MicroTom) plants were transformed using either a *Pro35S:GFP-SlMAP70-1* construct or an RNA interference (RNAi) construct that targets the *SlMAP70-1* gene (Supplemental Fig. S3A). As a high sequence similarity is found among the genes of MAP70-1 clade (Supplemental Fig. S3A), the expression of *SlMAP70-2* and *SlMAP70-3* was also slightly reduced in *SlMAP70-1* RNAi lines (Supplemental Fig. S3B). In transgenic tomato *Pro35S:GFP-SlMAP70-1* lines, GFP-SlMAP70-1 localized to filaments that were sensitive to oryzalin treatment (Fig. 2A), a drug-preventing microtubule polymerization (Morejohn et al. 1987), confirming a microtubule localization. Plants with elevated levels of *SlMAP70-1* exhibited elongated fruit shapes, while fruits with the knocked-down expression of *SlMAP70-1* were flatter (Fig. 2B; Supplemental Fig. S3, B and C). The phenotype was consistently observed in multiple independent transgenic lines (Fig. 2B). Quantitative and statistical analysis revealed that fruit length was increased in *SlMAP70-1* overexpressing lines (denoted as OE), and oppositely, in *SlMAP70-1* RNAi lines fruit length was reduced (Fig. 2C), resulting in increased and reduced fruit shape indices (as indicated by the aspect ratio), respectively, compared to wild type (WT). The *SlMAP70-1* RNAi construct was also transformed into another tomato cultivar, Ailsa Craig (AC), and the effect of RNAi was further confirmed by immunoblotting with a SlMAP70-1 antibody (Supplemental Fig. S4, A to C). As observed in MicroTom, transgenic AC fruits with knocked-down *SlMAP70-1* expression were flatter than WT fruits (Supplemental Fig. S4A), indicating that the function of *SlMAP70-1* during fruit shape formation is likely conserved in different tomato varieties.

To address potential functional redundancies, loss-of-function mutants of different *SlMAP70* members were generated using the CRISPR/Cas9 technique (Supplemental Fig. S5, A to D). Target sites that are conserved in the MAP70-1 clade were selected, to knock out multiple genes in one transformation (Supplemental Fig. S5, A and B). In the end, different combinations of *slmap70* mutants were obtained. The *slmap70-1* and *slmap70-2* single mutants resulted in reduced shape indexes, and the reduction in fruit length was further enhanced in *slmap70-1 slmap70-2* double and *slmap70-1 slmap70-2 slmap70-3* triple mutants (Fig. 2, D and E). On the other hand, *slmap70-4 slmap70-5* double mutants did not exhibit significant changes in fruit phenotypes (Fig. 2, D and E), indicating that *SlMAP70-1*, *SlMAP70-2*, and *SlMAP70-3* are likely the major players in regulating tomato fruit shape and elongation. However, the *slmap70-1 slmap70-2 slmap70-3* triple mutant also showed a defect in plant reproduction and produced few seeds (Fig. 2D); thus, the *slmap70-1 slmap70-2* double mutant was selected for further fruit shape studies.

SlMAP70 proteins have a global effect on organ and cell morphogenesis

In addition to changes in fruit shape, cell morphological changes were observed in *SlMAP70-1* transgenic plants (Fig. 3A; Supplemental Fig. S6A). Although the average cell area was not changed in different backgrounds, cell circularity (a measure for cell shape complexity with a value of 1 representing a circle and values approaching 0 indicating increasingly complex shapes) was reduced in both leaf epidermal pavement cells and mature fruit endocarp cells of *SlMAP70-1* OE lines but increased in *SlMAP70-1* RNAi lines, respectively (Fig. 3, B and C). Cell lobe numbers were not statistically different between WT cells and the *SlMAP70-1* OE or RNAi cells, but the average lobe length was significantly shorter in *SlMAP70-1* RNAi lines (Fig. 3, D and E). Similar phenotypes were also observed in cotyledon cells of *SlMAP70-1* transgenic lines (Supplemental Fig. S6, A and B). In tomato seedlings, the hypocotyls (as well as hypocotyl pavement cells) were elongated in *SlMAP70-1* OE lines but shortened in *SlMAP70-1* RNAi and *slmap70-1 slmap70-2* mutant lines (Supplemental Fig. S6, A and B). These results suggest that the function of *SlMAP70* in cell and tissue morphogenesis is likely conserved in different cell types.

SlMAP70 proteins alter microtubule rearrangements during early fruit development

The arrangement of microtubules has a direct impact on cell expansion and anisotropy of growth. We thus suspected that the altered cell circularity (Fig. 3A) and fruit shape (Fig. 2) in *SlMAP70-1* transgenic lines are likely linked to changes in microtubule organization regulated by SlMAP70 proteins. To test this hypothesis, we first studied the organization and dynamics of microtubules during fruit development using a transgenic tomato line expressing the GFP-MAP65-1 (Fig. 4; Supplemental Fig. S7), which was used as a microtubule marker in previous studies (Riglet et al. 2020). We also attempted to generate lines expressing other microtubule markers (e.g. RFP-TUA5), but these fusion proteins have a dramatic impact on tomato reproduction and no transgenic seeds were obtained. Before further analyses, we validated that GFP-MAP65-1 colocalized with the microtubule marker RFP-TUA5 (Supplemental Fig. S7, A and B) and that expression of GFP-MAP65-1 did not affect tomato fruit size and shape (Supplemental Fig. S7, C and D), suggesting that GFP-MAP65-1 is a suitable marker for analysis of CMTs in tomato fruits.

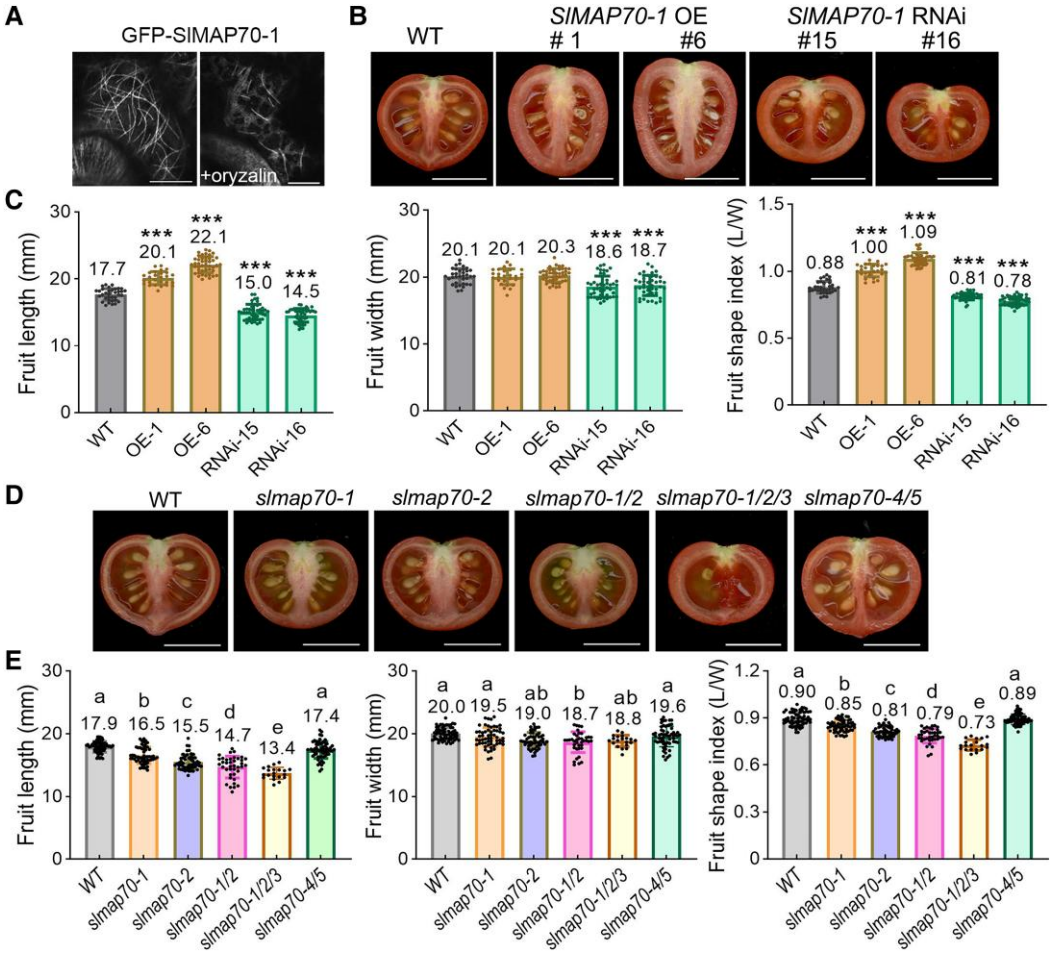

Figure 2. SlMAP70 proteins affect fruit morphogenesis. **A)** Subcellular localization of GFP-SlMAP70-1 in tomato leaf pavement cells. Bars: 10 μm. **B, C)** Effects of *SlMAP70-1* expression on fruit shape. Bars: 1 cm. The error bars and asterisks in the graph indicate the standard errors and significant differences compared with the WT evaluated by Tukey's test (***$P < 0.001$). **D, E)** Fruit shape of *SlMAP70* mutants by CRISPR/Cas9. The lowercase letters indicate the difference of $P < 0.05$ by Tukey's test. More than 20 fruits from 3 to 4 plants were analyzed; each dot represents a measurement of a fruit. Bars: 1 cm. The *slmap70-1/2* refers to *slmap70-1 slmap70-2* double mutant, *slmap70-1/2/3* refers to *slmap70-1 slmap70-2 slmap70-3* triple mutant, and *slmap70-4/5* refers to *slmap70-4 slmap70-5* double mutant.

Microtubule structure is influenced by space confinement and mechanical pressure (Colin et al. 2020). It thus is essential to compare microtubule rearrangements in cells with similar morphology. Cells from different fruit tissues were checked (Fig. 4A), and we found only cells from the endocarp tissue are suitable for live cell imaging. In other fruit tissues, cells are either very small or uniformly shaped (e.g. exocarp pavement cells) or not easily accessible by conventional light microscopy (e.g. placenta and mesocarp cells) (Fig. 4B). In endocarp tissue, the average cell area increased slightly at the late ovary development stages (−3 to 0 d) and early fruit development stages (0 to 5 d), and their cell circularity remained the same at these stages (Fig. 4, C to E). Therefore, cells in fruit endocarp tissue were chosen for study.

The anisotropy scores were calculated as described before (Boudaoud et al. 2014). A score of 0 represents no order (all filaments arranged in different directions) and 1 represents perfect order (all filaments in the same direction). Analysis of GFP-MAP65-1 lines revealed that during early fruit development, the values of microtubule anisotropy did not change from Days −3 to 0 but decreased significantly after Day 0 (24 h after pollination), indicating that microtubules became less ordered at this period (Fig. 4, F and G). In the *slmap70-1 slmap70-2* mutant, the changes of CMTs exhibited a similar pattern in general (Fig. 4, F and H) but appeared to be more ordered from Day 0 when compared to the WT at the same stage (Fig. 4, F and I). These results indicated that microtubules rearranged dramatically during early fruit development and that such precise regulation of microtubule patterning could be mediated by SlMAP70 proteins, contributing directly to microtubule arrangement and may directly affect cell morphogenesis during early fruit development.

Next, endocarp cells in the middle region of young fruit at the Day 0 stage were selected for further studies (Fig. 5A). Laser scanning confocal microscopy revealed that endocarp cell circularity in *slmap70-1 slmap70-2* mutant lines was

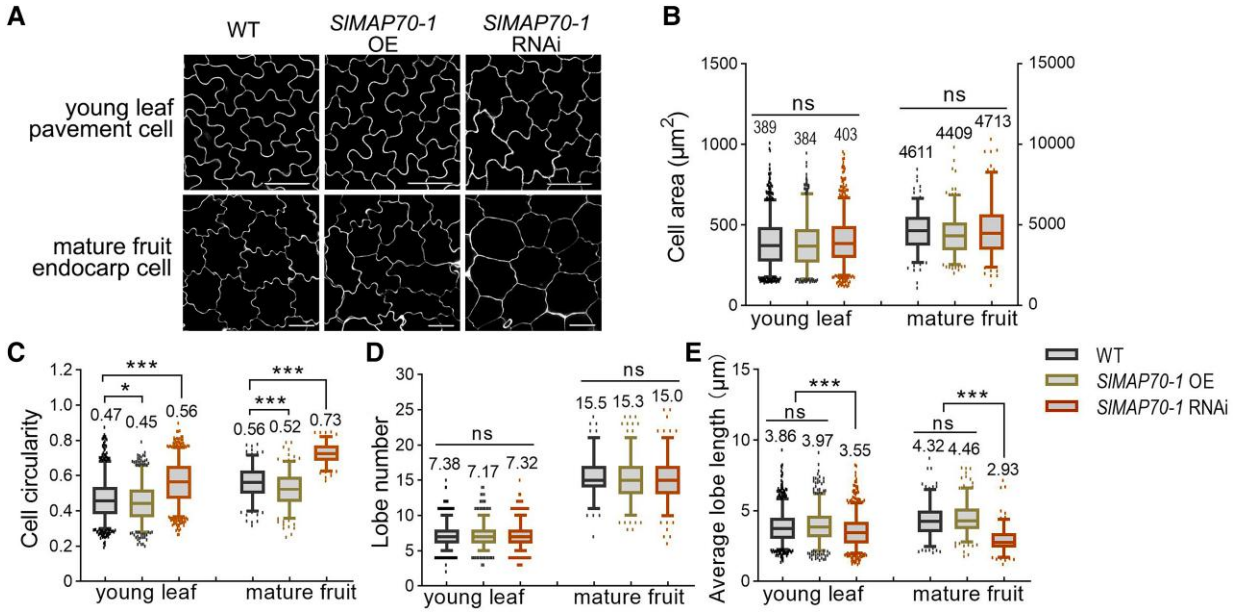

Figure 3. Cell shape analysis with aberrant expressions of *SlMAP70-1*. **A)** Leaf pavement cells of 10-d-old seedlings after germination and endocarp cells of mature fruits. Cell contours were visualized by propidium iodide (PI) staining. Bars: 50 μm for endocarp pavement cells. Bars: 25 μm for young leaf pavement cells. **B to E)** Quantification of cell lobe characters (number and average length), cell size (area), and shape circularity. Overexpression of *SlMAP70-1* caused more irregular cell morphology, and the downexpression of *SlMAP70-1* led to more circular cells. More than 180 cells from 6 confocal images of 3 different plants were analyzed; each dot represents a measurement of a cell. ns, no significance; $^{*}P < 0.05$; $^{**}P < 0.01$; $^{***}P < 0.001$ by Tukey's test with a 95% confidence interval. The center line of boxplot indicates median value.

increased, while it was reduced in *SlMAP70-1* OE lines compared to the WT (Fig. 5, B and C). Interestingly, the average anisotropy score of CMT was also increased (more ordered) in *slmap70-1 slmap70-2* mutant lines but reduced in *SlMAP70-1* OE lines (Fig. 5, B and D). Similar to the *SlMAP70-1* OE lines, transgenic tomato overexpressing both *SlMAP70-1* and *SlIQD21a* (which have more elongated fruits, discussed later) also exhibited reduced cell circularity and CMT anisotropy (Fig. 5, B to D).

In *Arabidopsis*, it is established that cells with a high circularity often exhibit low microtubule anisotropy, so cells can expand isotropically in random directions. However, an opposite effect was found in tomato endocarp cells, where increased CMT order was found in cells of the *slmap70-1 slmap70-2* mutant with a high circularity. The reason for such difference is not clear; we hypothesize that the tissue organization in tomato fruits is more complicated than in *Arabidopsis*, so the space constraints and mechano-pressure among cells are different. Alternatively, such variation might be attributed to the difference in cell type used for tomato fruit and *Arabidopsis*.

The anisotropy measurements, however, only indicate the arrangement of individual microtubule filaments within each cell but are not very useful to determine the relationship between microtubule pattern and cell shape at a larger scale. Therefore, we also quantified the orientation angle of microtubules at the Day 0 stage of fruit development (Fig. 5B). Measurements close to 90° indicate most microtubule arrays within a cell are vertically organized (parallel to the growth direction), while transverse microtubules are measured close to 0° or 180° (Fig. 5A). In the *slmap70-1 slmap70-2* mutant, endocarp cells exhibited a network of microtubule arrays that had no directional preference at the supracellular level compared to the WT (Fig. 5, E and F). In contrast, transverse microtubule arrays were more pronounced in the endocarp cells of *SlMAP70-1* OE and *SlMAP70-1 SlIQD21a* double OE lines (Fig. 5, G and H).

According to these observations, we suggested that microtubules are more ordered in *slmap70-1 slmap70-2* mutant at the single-cell level (Fig. 5D), but the average CMT orientation varies from cell to cell at the supracellular level (Fig. 5F), so each cell may expand in a different direction, generating flatter/round fruits. In contrast, microtubules are mostly transversely oriented in elongated fruits, restricting the cell lateral expansion and promoting cell elongation along the longitudinal axis (e.g. *SlMAP70-1* OE). It is also worth pointing out that these studies were performed using the endocarp tissue. Whether the cells of exocarp tissue exhibit similar variation of CMT organization is not clear.

SlMAP70s interact with SlIQD21 proteins

As microtubule structure and dynamics are precisely regulated, such rapid reorientation of CMT arrays during fruit development may require SlMAP70 proteins to act in concert with other microtubule regulators. Therefore, the molecular basis of SlMAP70-regulated fruit morphogenesis and microtubule arrangement was studied.

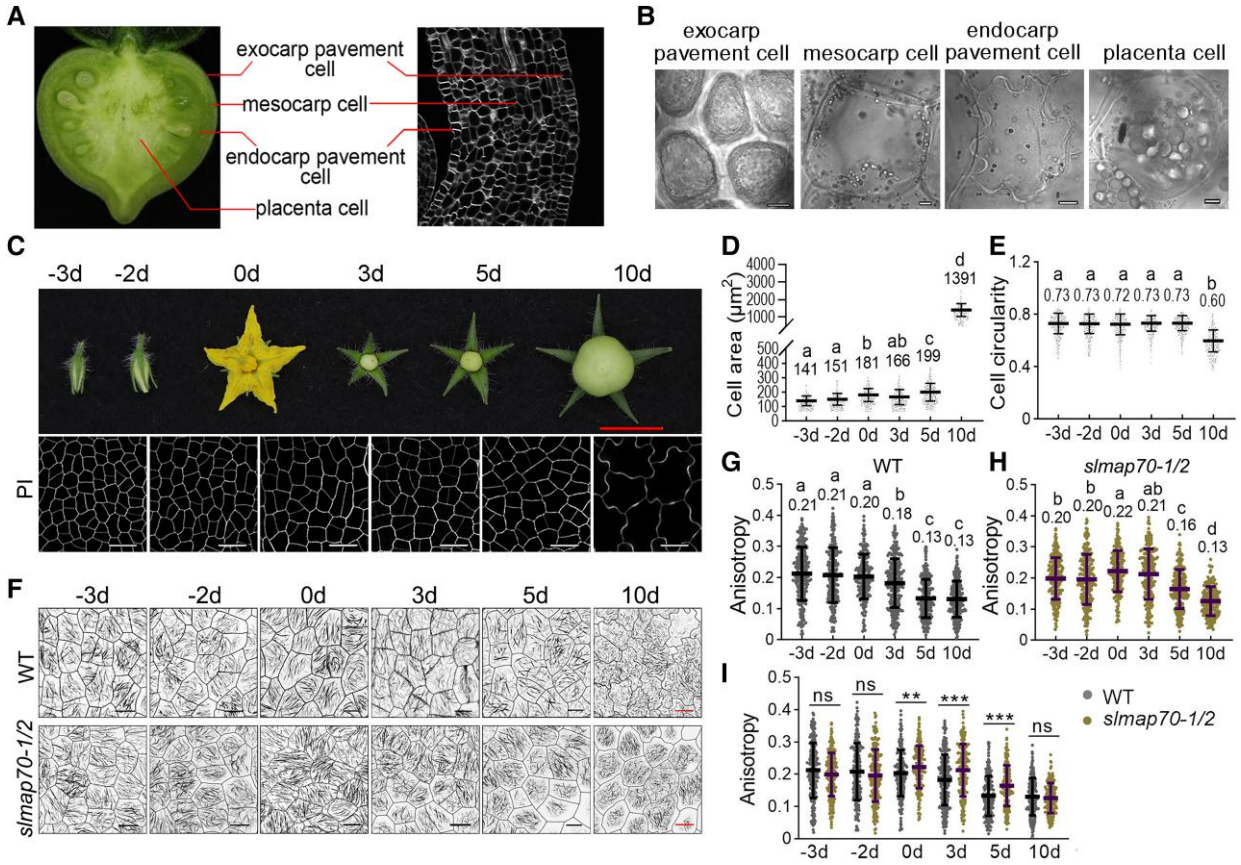

Figure 4. CMT arrangement in tomato fruit cells during fruit growth. **A)** A demonstration of different fruit tissues that were studied. **B)** Images of fruit cells from the tissues are shown in **A)**. Bars: 10 μm. **C)** Endocarp pavement cells of tomato fruits at different developmental stages. PI, propidium iodide. Red bar: 1 cm. White bars: 25 μm. **D, E)** Quantitative analyses of endocarp pavement cell size and circularity of the WT fruits at different development stages. The letters indicated a significant difference by Tukey's test ($P < 0.05$). Values are given as the mean ± SD of more than 300 cells from 6 confocal images of 3 different plants. **F)** The organization of CMT arrays (labeled by GFP-MAP65-1) was analyzed at various development stages in the WT and *slmap70-1 slmap70-2* double mutant. Black bars: 10 μm. Red bars: 25 μm. **G to I)** Quantitative analyses of CMT anisotropy for the indicated genotypes at the different development stages. The lowercase letters in **G)** and **H)** indicate the difference of $P < 0.05$ by Tukey's test. The asterisk in **I)** indicates the difference between WT and *slmap70-1 slmap70-2* double mutant at the same point by *t*-test with $P < 0.01$ for ** and $P < 0.001$ for ***. Values are given as means ± SD of more than 180 cells from 9 confocal images of 3 different plants.

Using SlMAP70-1 as a bait, SlIQD21a (also named SUN10 from the tomato genome annotation) was identified as a putative interaction partner from a Y2H screen. Public expression data (Tomato Genome Consortium 2012, http://ted.bti.cornell.edu/) indicated that *SlIQD21a* is expressed at high levels in early-developing fruits and young leaves (Supplemental Fig. S8A), similar to the expression pattern of *SlMAP70-1* (Fig. 1B). Analysis of SlIQD21a subcellular localization showed that GFP-SlIQD21a localizes to CMTs, as indicated by colocalization with RFP-TUA5 (Supplemental Fig. S8B).

Coexpression of *RFP-SlIQD21a* and *GFP-SlMAP70-1* in *N. benthamiana* leaf pavement cells showed clear colocalization in a continuous pattern along the CMTs (Fig. 6A). Protein interaction between SlMAP70-1 and SlIQD21a was validated using bimolecular fluorescence complementation (BiFC) and coimmunoprecipitation (Co-IP) (Fig. 6, B and C), confirming SlIQD21a as a bona fide SlMAP70-1 interactor. Such interaction is likely conserved among SlMAP70 homologs, as indicated by Y2H interaction and colocalization assays between the five tomato MAP70 isoforms with SlIQD21a (Fig. 6D; Supplemental Fig. S9 A to D).

In tomato, 33 SUN/IQD family members were identified, and they are divided into 3 main clades each containing several subclades according to phylogenetic analysis in comparison to *Arabidopsis IQD* genes (Huang et al. 2013). To test if SlMAP70-1 interaction is conserved among SlIQDs, we cloned tomato *SUN/IQD* genes from the distinct phylogenetic subclades, including *SUN12/SlIQD12b*, the closest homolog to the well-known fruit shape regulator *SUN1* (Xiao et al. 2008; Huang et al. 2013), and *SUN16/SlIQD21b*, the closest homolog to *SlIQD21a* (Huang et al. 2013). In addition, we also selected *SUN29/SlIQD1*, *SUN31/SlIQD5*, *SUN23/SlIQD23*, and *SUN32/SlIQD25*. When transiently expressed in *N. benthamiana*, all tested GFP-SlIQD fusion proteins localized to microtubules labeled with RFP-TUA5

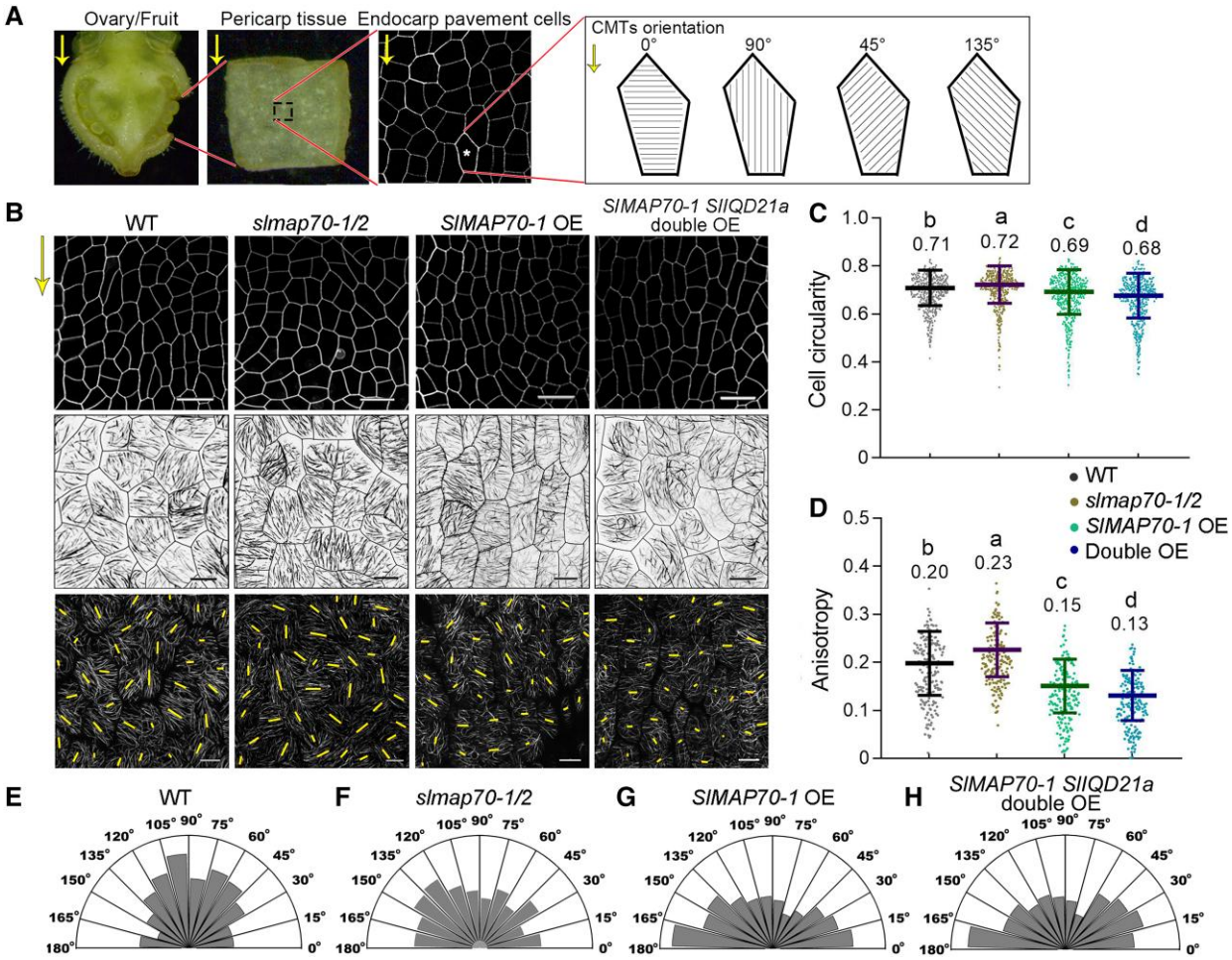

Figure 5. SlMAP70-1 and SlIQD21a proteins regulate CMT arrays at the early fruit development stage. **A)** A demonstration of sample preparation for imaging fruit endocarp cells. The average microtubule angle was valued between 0° and 180°. 0° is perpendicular to the proximo-distal direction (yellow arrows) of the fruit sample. **B)** Analyzing endocarp epidermal cell shape (top) and microtubule organization (middle) at fruit development stage Day 0 (the day of anthesis after manual pollination for 24 h). The CMT arrays in all genotype lines were labeled by GFP-MAP65-1. The length and orientation of yellow lines (bottom) represent the anisotropy and orientation of the CMT arrays in each cell that are quantified with FibrilTool. Bars for cells: 25 μm. Bars for CMT: 10 μm. **C, D)** Quantitative analysis of the cell circularity and CMT anisotropy in **B)**. The lowercase letters indicate the difference of $P < 0.05$ by Tukey's test. More than 450 cells from 4 ovaries per genotype were analyzed. **E to H)** Quantitative analyses of the percentage of CMT orientation (angles from 0° to 180°) in **B)** for the indicated genotypes at Day 0 stages. More than 180 cells were analyzed from 6 ovaries per genotype were analyzed.

(Supplemental Fig. S8B). Interaction of SlMAP70-1 in Y2H assays was observed only for SlIQD21a and SlIQD21b (Fig. 6E). These findings suggest that SlIQD proteins differentially interact with SlMAP70-1 protein and that interaction may be limited to a few SlIQD proteins.

SlIQD21a regulates tomato fruit shape

A previous study reported that the tomato *sun* variant showed a long fruit phenotype, which is attributed to higher expression levels of *SUN1* (Xiao et al. 2008). To more broadly test the function of tomato IQDs in fruit formation and shape establishment, we selected 3 of the SlIQDs for further functional analysis. They included SlIQD21a, the SlMAP70s interacting protein, SlIQD12b, the closest homolog of SUN1 (Xiao et al. 2008; Huang et al. 2013), and SlIQD1, which shares sequence similarity with *Arabidopsis* IQD2 involved in root and leaf cell morphogenesis (Zang et al. 2021). Overexpression constructs of these genes were transformed into tomato plants.

As in *N. benthamiana*, all 3 GFP-SlIQD variants labeled filamentous structures in tomato leaf pavement cells, and the oryzalin treatment of GFP-SlIQD1 expressing cells confirmed these structures are microtubule related (Supplemental Fig. S10A). Interestingly, fruits from these transgenic plants showed different shapes. *SlIQD1* OE lines did not display significant changes in fruit size and shape compared to the WT, while the fruits from both *SlIQD12b* and *SlIQD21a* OE lines were elongated (Fig. 7, A and B; Supplemental Fig. S10, B and C). In *SlIQD12b* transgenic plants, fruits were extremely elongated (Supplemental Fig. S10, B and C), similar to

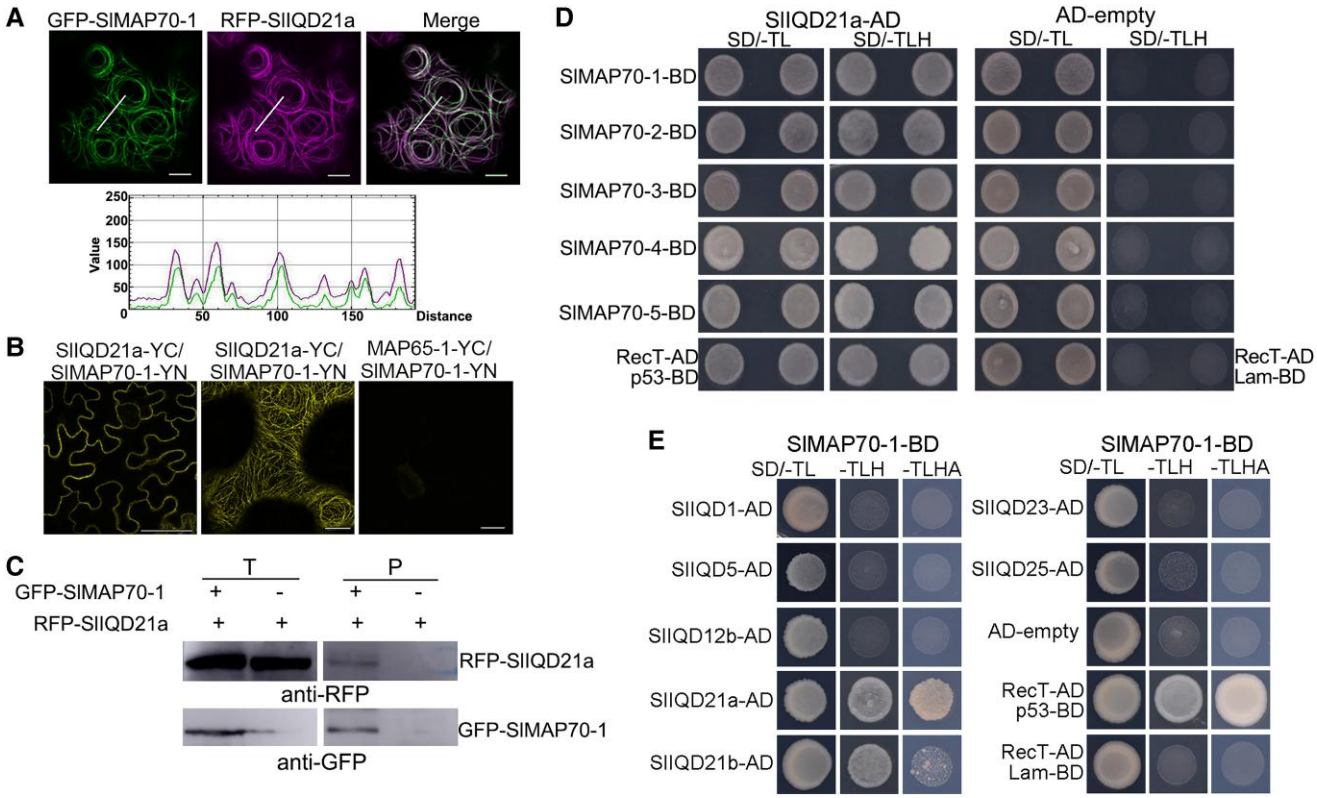

Figure 6. SlMAP70 proteins interact with tomato SlIQD21a. **A)** RFP-SlIQD21a colocalized with GFP-SlMAP70-1 in *N. benthamiana* leaf epidermal cells. The GFP signal of SlMAP70-1 fusion protein along the white line superposed with the RFP signal of SlIQD21a fusion protein. Bars: 10 μm. **B)** BiFC assays of protein interaction between SlMAP70-1 and SlIQD21a in *N. benthamiana* leaf epidermal cells. YFP fluorescence was visible along the CMT filamentous structure. The N-terminal (YN) and C-terminal fragments (YC) are fused to proteins of SlMAP70-1 and SlIQD21a, respectively. MAP65-1-YC served as negative controls. Bars: 10 μm. **C)** GFP-Trap–based Co-IP assay of GFP-SlMAP70-1 and RFP-SlIQD21a; the blot was detected using an RFP antibody. RFP-SlIQD21a was only found in the pellet fraction in the presence of GFP-SlMAP70-1. **D)** Y2H analysis indicates SlIQD21a interacts with all SlMAP70 proteins. p53 + RecT indicates positive control, and Lam + RecT indicates negative control. **E)** Y2H assay of interactions between SlMAP70-1 and other selected SlIQD proteins. For Y2H, all the strains could grow on synthetic dropout media without Trp and Leu (SD/-TL), whereas only positive strains could grow on SD/-LTH (SD/-Trp/-Leu/-His) media, and strong positive strains also could grow on SD/-LTHA (SD/-Trp/-Leu/-His/-Ade).

phenotypes reported for *SUN1* overexpression plants (Xiao et al. 2008). Fruits from the *SlIQD21a* transgenic plants exhibited only mild elongation (Fig. 7, A and B), similar to those in *SlMAP70-1* overexpressing plants (Fig. 2, B and C).

Therefore, we hypothesized that SlIQD proteins may contribute to fruit shape formation differentially through specific molecular mechanisms. We also generated transgenic tomato lines of *sliqd21a* knock-out mutant by CRISPR/Cas9 technique (Supplemental Fig. S11, A and B), and these *sliqd21a* mutants exhibited an observable flatter fruit shape phenotype compared to WT plants (Fig. 7, A and B). As SlIQD21a and SlMAP70-1 interact and exhibit similar fruit-shape phenotypes, we hypothesized that both proteins may function together in microtubule organization, and coordinately regulate fruit shape.

Coexpression of *SlIQD21a* and *SlMAP70-1* further enhances fruit elongation

To further dissect the proposed joint role of *SlMAP70-1* and *SlIQD21a* in fruit shape regulation, we crossed *SlMAP70-1* OE lines with *SlIQD21a* OE lines, generating stable tomato plants expressing both constructs (Supplemental Fig. S12, A to C). Compared to the plants overexpressing *SlMAP70-1* or *SlIQD21a* alone, the *SlMAP70-1 SlIQD21a* double OE lines showed an enhanced fruit elongation phenotype and higher fruit shape index (Supplemental Fig. S12B). According to the gene expression data (Fig. 1B; Supplemental Fig. S8A), we hypothesized that both *SlMAP70-1* and *SlIQD21a* may exert their function from early fruit set stages, which may determine the shape of fruits. Therefore, ovaries right after anthesis were studied at both tissue and cell level.

Results showed that all genotypes displayed significant changes in ovary shape compared with WT tomato (Fig. 7, C and D). *SlMAP70-1* RNAi line exhibited a flatter ovary with decreased ovary length and no changes in ovary width compared to the WT. In contrast, the *SlMAP70-1* overexpression line exhibited a slender ovary with a significant increase in ovary length and a decrease in width, similar to the phenotype of *SlIQD21a* OE lines (Fig. 7D). Cooverexpression of *SlIQD21a* and *SlMAP70-1* further enhanced ovary elongation

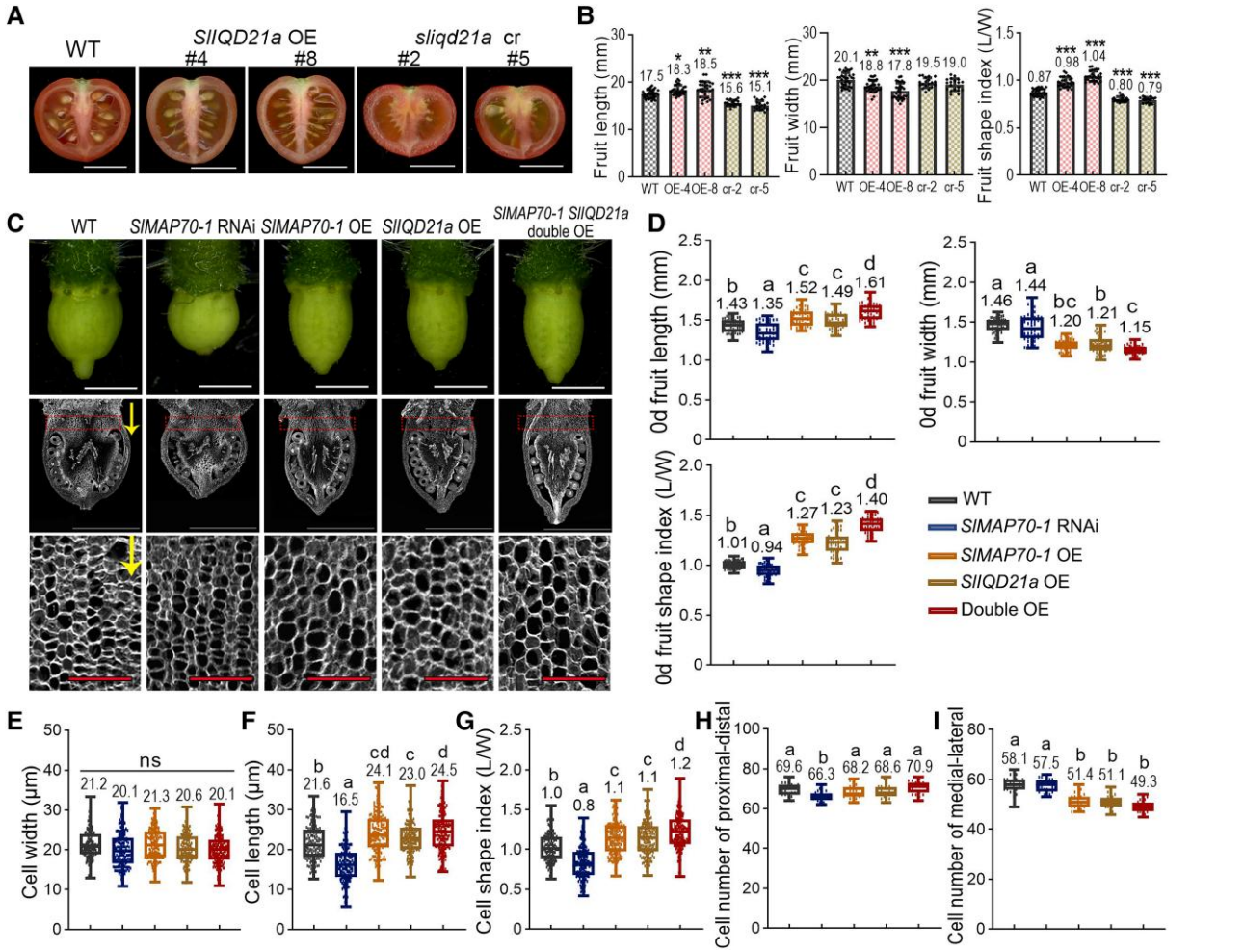

Figure 7. Enhancing the ovary elongation by *SlIQD21a* coexpressed with *SlMAP70-1*. **A)** The phenotype of mature fruits of *SlIQD21a* OE and *sliqd21a* mutant lines. Bar: 1 cm. **B)** Analysis of mature fruit shape characters of *SlIQD21a* OE and mutant transgenic lines compared to WT, respectively. cr represent *sliqd21* mutants by CRISPR/Cas9; OE represent *SlIQD21a* overexpressing line. Data are shown as mean ± SD, $n > 20$. ***$P < 0.001$; **$P < 0.01$; *$P < 0.05$ by Tukey's test. **C)** Microscope images of anthesis-stage ovaries (top) and paraffin sections along the longitudinal axis (middle). Images in the bottom row are cells from the proximal end (red dotted rectangle) of ovaries with high magnification. Yellow arrows indicate the proximal-distal direction of ovary growth. White bars: 1 mm. Red bars: 0.1 mm. **D)** Statistical analysis of 0-d fruit length, width, and aspect ratio in **C)**. More than 40 ovaries at anthesis from 3 plants for each genotype were analyzed; each dot represents a measurement of an ovary. **E to G)** Statistical analysis of cell length, width and aspect ratio in the parenchyma zone (red dotted rectangle) of anthesis ovaries in **C)**. **H and I)** Statistical analysis of cell numbers along the proximal-distal and medial-lateral direction of whole ovaries in **C)**. More than 150 cells from 15 ovaries for each genotype were analyzed. The lowercase letters indicate the difference of $P < 0.05$ by Tukey's test. The center line of boxplot indicates median value.

and reduced ovary width (Fig. 7D), similar to the shape of mature fruits (Supplemental Fig. S12A).

An in-depth analysis of cell parameters at the proximal end (Fig. 7C, red rectangle) of the anthesis-stage ovaries was also characterized according to Wu et al. (2018). Cell width was not altered in all these transgenic plants (Fig. 7E), whereas cell length was significantly longer in all OE transgenic lines and shorter in the *SlMAP70-1* RNAi line (Fig. 7F) compared to WT, leading to changes in cell shape indexes (Fig. 7G). Cell number along the proximo-distal (longitudinal) axis decreased significantly in *SlMAP70-1* RNAi fruits (Fig. 7H), while cell number along the medial-lateral (horizontal) axis decreased significantly in all overexpression plants (Fig. 7I). These results suggest that the main roles of SlMAP70-1 and SlIQD21a in fruit elongation are to regulate cell expansion in the longitudinal direction and possibly also affect cell division from early ovary stages.

SlIQD21a and SlMAP70 affect microtubule stability to regulate microtubule patterning

So far, we showed that the SlMAP70 protein level and its interaction with SlIQD21a are essential for fruit elongation. Next, we moved on to study the exact effects of SlMAP70 proteins on microtubules using chemical treatment and analytical imaging methods. In *N. benthamiana* cells, coexpressing RFP-SlIQD21a and GFP-SlMAP70 proteins induced the formation of thick microtubule bundles and microtubule whorls were predominant (Fig. 6A; Supplemental Fig. S9).

Similar microtubule circles were also observed in tomato endocarp cells of *SlMAP70-1* OE and *SlMAP70-1 SlIQD21a* double OE lines (Supplemental Fig. S13). Such microtubule patterns had been reported in a few previous studies, but their biological relevance was unclear (Kirik et al. 2007; Ren et al. 2017). From a biophysical perspective, it is suggested that microtubule whorls are induced by local interactions between each filament (e.g. proteins inducing microtubule bundling) and result from a joint effect of microtubule collision followed by a reptation-like motion of single microtubules (Sumino et al. 2012).

To gain quantitative insights into the changes in microtubule organization, we measured the length of the microtubule filaments. Long filaments were very abundant when expressing *SlMAP70-1* or both *SlMAP70-1* and *SlIQD21a*, but their occurrence was reduced in the *slmap70-1 slmap70-2* mutant (Fig. 8, A and B; Supplemental Fig. S14, A and B). This abnormal behavior may favor the formation of microtubule whorls, which consisted of very long microtubule filaments, in either a clockwise or anticlockwise direction.

To determine the effect of *SlIQD21a* and *SlMAP70-1* expression on microtubule dynamics, time-lapse studies were performed using a frame-subtraction approach (Lindeboom et al. 2013; Smertenko et al. 2020). Here, microtubule growth (polymerization) was pseudocolored in red, and microtubule shrinkage (depolymerization) was pseudocolored in cyan. In control cells expressing GFP-β-Tubulin6 (GFP-TUB6), both events were frequently observed, while microtubule dynamics appeared to be reduced in the presence of SlIQD21a or SlMAP70-1 (Fig. 8C). In cells coexpressing *SlIQD21a* and *SlMAP70-1*, microtubules appeared static as little growth or shrinkage was observed in the processed images (Fig. 8C; Supplemental Movies S1 and S2). Thus, these results suggest that SlIQD21a and SlMAP70-1 stabilize microtubules and that this effect is further enhanced when both proteins are coexpressed.

Different transgenic tomato seedlings were treated with 300 nM oryzalin (Fig. 8D), which prevents de novo microtubule polymerization and inhibits plant growth (Morejohn et al. 1987; Yang et al. 2020). Root growth without oryzalin treatment was similar among different genotypes. However, tomato seedlings overexpressing *SlMAP70-1* or both *SlMAP70-1* and *SlIQD21a* were more resistant to oryzalin treatment, exhibiting longer roots after oryzalin treatment, while RNAi plants with reduced expression of *SlMAP70-1* were more susceptible (Fig. 8E).

To further confirm the microtubule-stabilizing effect of SlMAP70-1 and SlIQD21a, we used a stable transgenic *N. benthamiana* plant expressing *RFP-TUA5* (Guo et al. 2023), so the density of RFP-TUA5 labeled microtubules can be quantified. In control leaf pavement cells, high-concentration oryzalin disrupts microtubules within 10 min, while most microtubules were depolymerized after 20 min treatment (Fig. 8, F and G). But this effect was less prominent in the presence of overexpressed *SlMAP70-1* and *SlIQD21a*, especially for those coexpressed cells, in which intact microtubules still could be observed after oryzalin treatment for 40 min (Fig. 8, F and G). All these results support our conclusion that SlMAP70-1 and SlIQD21a likely regulate microtubule function through a stabilizing effect. We hypothesize that such a stabilization effect may perturb dynamic microtubule rearrangement in various cell types (Fig. 5; Supplemental Fig. S14) and may be directly attributed to the alteration in cell directional growth and fruit shape establishment.

In conclusion, we propose that SlMAP70 proteins and SlIQD21a contribute to microtubule stability, which may affect the rearrangement of CMTs and cell growth patterns underlying organ shape. SlMAP70 proteins interact with SlIQD21a (possibly other microtubule regulators) and maintain CMT reorganization during fruit development. Increasing the expression of *SlMAP70-1* or *SlIQD21a* stabilizes CMTs and affects CMT rearrangement at both cell and tissue levels. Such alterations favor cell expansion along the longitudinal direction, leading to longer fruits. Conversely, in the absence of *SlMAP70s*, although the CMT is more ordered at the cellular level, the average CMT angle of each cell varies dramatically at the supracellular level, thereby promoting cell growth in random directions and producing flatter fruits (Fig. 9).

Discussion

During the past years, genes encoding microtubule-binding proteins emerged as conserved trait loci for fruit shape regulation with important roles during domestication, as has been reported in tomato, cucumber, melon (*Cucumis melo*), peach (*Prunus persica*), and rice (Dou et al. 2018; Wu et al. 2018; Pan et al. 2020; Yang et al. 2020; Zhou et al. 2021). However, most of these studies were performed using forward genetics or population genetics approaches, and the in-depth molecular and cell biological insight has not been investigated. Early studies in model plants showed that MAPs regulate microtubule function in different ways and contribute to cell wall composition, cell polarity, and cell division. Understanding the molecular basis of these processes in fruit crops would certainly provide a powerful toolbox for fruit shape regulation in the future.

CMTs are aligned with maximal tensile stress in plant tissues and are required for maintaining anisotropic growth through guiding cellulose microfibril deposition (Robinson and Kuhlemeier 2018; Zhao et al. 2020). In *Arabidopsis*, the transverse organization of microtubules is often observed in elongating cells, such as hypocotyl tissues (Montesinos et al. 2020; Wang et al. 2020), so the CMT anisotropy is normally higher, and the average angle of CMT is normally perpendicular to the direction of cell expansion. However, the scenario is slightly different in tomato fruits. Using live-cell imaging of the microtubule organization of the endocarp cells, we found that the anisotropy of CMT networks was higher when *SlMAP70* functions were disturbed, generating

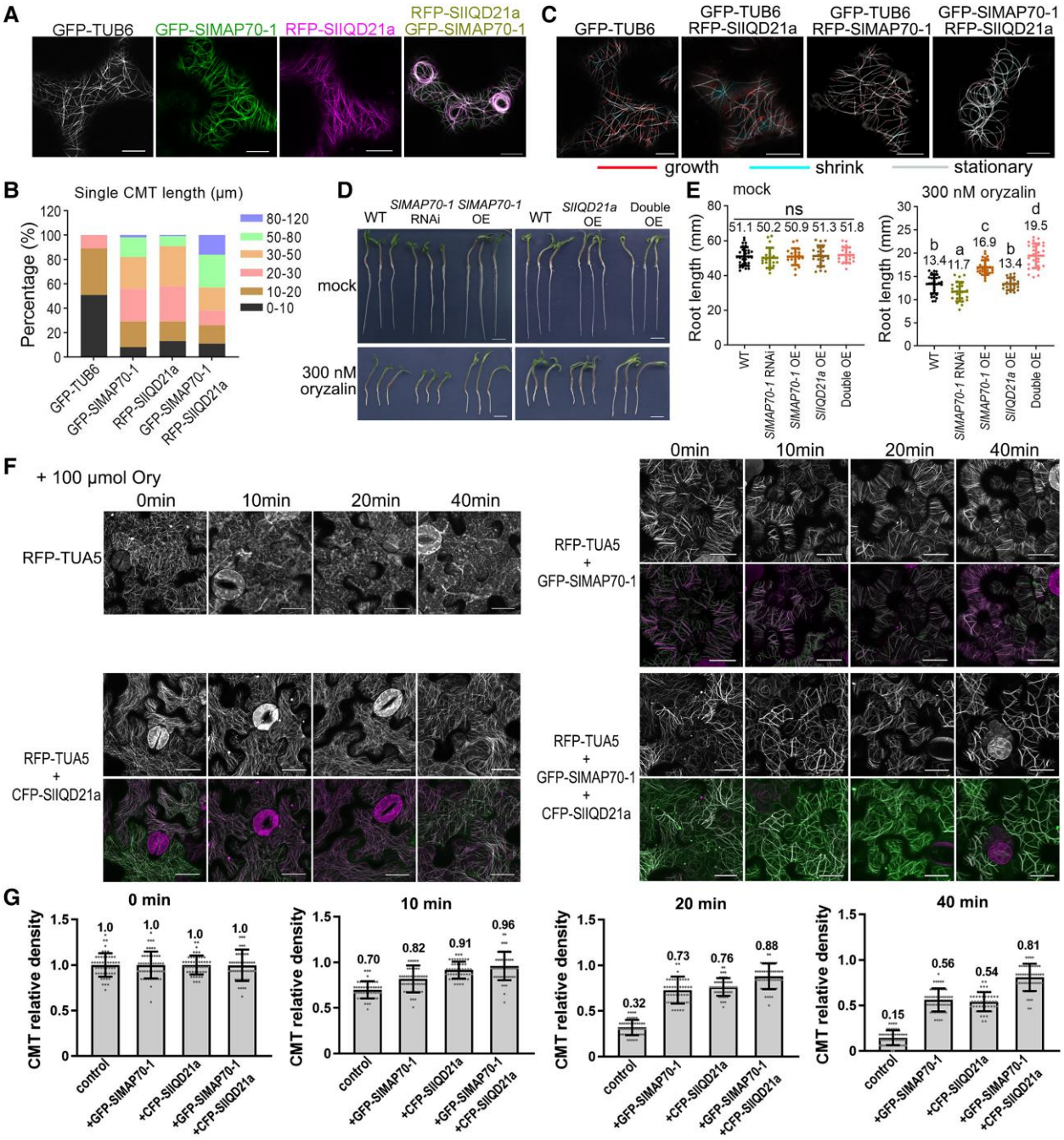

Figure 8. Overexpression of SlMAP70-1 and SlIQD21a proteins stabilizes microtubules in vivo. **A)** Coexpression of RFP-SlIQD21a and GFP-SlMAP70-1 resulting in long and bundling microtubules that are prone to form whorls-like arrays in *N. benthamiana* leaf epidermal cells. Bars: 10 μm. **B)** Statistical analysis of microtubule filament length in **A)**. The colors indicate the different length ranges of microtubule microfilaments. More than 100 filaments were analyzed. **C)** Representative confocal images from a time lapse in *N. benthamiana* leaf pavement cells showing dynamic microtubules in color and preexisting microtubules in gray. The red line indicates newly grown CMT, and the cyan line indicates shrink CMT. A total of 10 repeats were performed for each construct. The frames are separated by 45 s. Bars: 10 μm. **D)** Oryzalin treatment of different *SlMAP70-1* and *SlIQD21a* genotypes. Germinated seedlings were grown on a regular medium supplemented with 0 or 300 nM oryzalin for 4 d. Bars: 1 cm. **E)** Statistical analysis of root lengths of indicated genotypes under oryzalin treatment in **D)**. Different letters in dot plots indicate significance. Ns, no significant, $P < 0.05$ by Tukey's test. More than 20 seedlings per genotypes were analyzed. **F)** Effect of oryzalin on RFP-TUA5 labeled microtubules of *N. benthamiana* leaf pavement cells expressing CFP-SlIQD21a or GFP-SlMAP70-1. Representative confocal images were captured before and after treatment with 100 μM oryzalin (Ory) at different times, respectively. Bars: 10 μm. **G)** Quantification of CMTs after oryzalin treatment for 0, 10, 20, or 40 min, respectively. The vertical scale represents the relative ratio of CMT density across a fixed line (~25 μm). More than 40 lines from 20 cells of each sample were analyzed; each dot represents a CMT density value across a line.

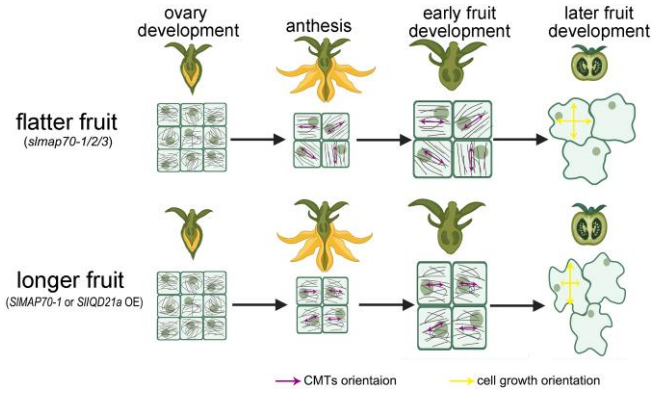

Figure 9. A schematic model of SlMAP70 and SlIQD21a proteins associating with microtubule orientation and cell growth to control the fruit shape. Tomato fruits were developed from ovaries after successful pollination, and their morphology is regulated by multiple *MAPs*, such as *SlMAP70* and *SlIQD21a*. During ovary development (as viewed from the endocarp), fruit cells are small and circular with little difference in the CMT array. In the *slmap70* mutant, the CMT array became more aligned at the single-cell level, but the average CMT angle varies from cell to cell at the tissue level, thereby promoting cell growth in the random direction and producing flatter fruits. By contrast, overexpressing *SlMAP70-1* or *SlIQD21a* reduces CMT anisotropy at the cellular level but is more uniform across the whole tissue, which resulted in longer fruit.

cells with increased circularity and flatter fruits. While in *SlMAP70-1* overexpressing plants, elongated fruits, reduced cell circularity and CMT anisotropy were observed (Fig. 5, B to D). It is not clear why this result is different from the established model in *Arabidopsis*, but we hypothesize that this is likely because the tissue complexity of tomato fruit is different from *Arabidopsis*. For example, previous works showed that CMTs reorganize in parallel bundles in the presence of mechanical stresses (Zhao et al. 2020), the mechano-strength among fruit pericarp cells is likely stronger in the *slmap70-1 slmap70-2* mutant, so the effect of mechanics-induced CMT organization is more dominant. On the other hand, the loss of *SlMAP70s* may also influence cell wall stiffness, which in turn affects microtubule behavior. Other possibilities may also exist, which would be very interesting for future investigations. Interestingly, the fruit epidermis is known as a load-bearing tissue and constrains fruit cell enlargement (Thompson et al. 1998; Bargel and Neinhuis 2005), so the behavior of CMT in exocarp and endocarp might be different. Unfortunately, the organization of CMT in other cell types was not studied here due to technical difficulties.

In addition, an early study also noticed that for the shape formation and anisotropic expansion of a tridimensional multicellular organ, cellulose microfibril alignment among cells at the tissue level is more important than the organization of microfibrils at the single cell level (Baskin 2005). Similarly, the microtubule orientation at the supracellular level also seems important to control the shape of tomato fruits. In *SlMAP70-1* and *SlIQD21a* overexpression lines, microtubules are preferably reorganized into transversely oriented arrays that restrict fruit cell growth orientation during ovary development (Fig. 9), generating elongated fruits. While in the *slmap70-1 slmap70-2* mutant, although each cell has a higher ordered CMT that facilitates directional cell expansion, the average CMT angle differs significantly among the cells, so each cell may grow in a different direction, generating flatter/round fruits. However, other factors, such as the direction of cell division and cell proliferation, may also contribute to fruit shape formation. These processes are also likely influenced by microtubule organization and dynamics but were not studied here.

SUN1 protein, also known as SlIQD12, was reported to localize to microtubules and regulate fruit shape and cell number by altering microtubule structure during cell division. Similarly, many other IQDs were reported to modulate fruit shapes by impacting cell division (Wu et al. 2011; Duan et al. 2017). Recent studies of *Arabidopsis* suggested that IQD6–8 proteins can recruit POK and PHGAP proteins at the cortical division zone (CDZ) to facilitate PPB formation, determining the division plane in plants (Schaefer et al. 2017; Kumari et al. 2021). So far, we have no direct evidence to suggest that SlIQD21a participates in PPB formation in tomato, but its interaction with SlMAP70 proteins that are localized at PPB structures in dividing cells (Fig. 6; Supplemental Fig. S2) may imply that SlIQD21a has the function on CDZ formation and cell division (as IQD6–8 reported in *Arabidopsis*). This will be an interesting topic for future studies.

Taken together, we studied the dynamics of microtubules in tomato fruits and identified candidates for fruit shape formation. Overexpressing *SlMAP70-1* promotes microtubule stabilization and reduces cytoskeletal dynamics that correspond with the formation of elongated fruits. The loss of function of *SlMAP70s* has the opposite effect confirming that SlMAP70s are important regulators of tomato fruit shape. We further demonstrate that SlMAP70 proteins interact with members of the tomato IQD family, in particular with SlIQD21a and related proteins, thereby linking functions of these 2 plant-specific families of MAPs. Both *SlMAP70-1* and *SlIQD21a* genes exhibit a high level of expression in young fruits and may regulate fruit shape formation jointly from the early stages of anthesis. It was also reported in a recent transcriptomic study that a number of microtubule-regulating genes, such as *SlIQD21a*, are highly expressed in a tomato cultivar (*fs8.1*) that has longer fruits (Chen et al. 2023). These findings on microtubule functional regulation may provide a powerful approach for fruit shape regulation in fruit crops in the future.

Materials and methods

Gene cloning and plasmid construction

For the RNAi construct of *SlMAP70-1*, a gene-specific fragment (472-bp) of *SlMAP70-1* (Supplemental Fig. S3A) was cloned into the pHellsgate8 vector using LR Clonase. For

the CRISPR/Cas9 constructs of *slmap70s* and *sliqd21a*, the target sequences of *SlMAP70* genes and *SlIQD21a* were designed using the online CRISPR-P2.0 web tool (http://crispr.hzau.edu.cn/CRISPR2/) and fused with 2 single-guide RNA (sgRNA) expression cassettes into pTX vector by assembly clone using BsaI restriction sites (Supplemental Figs. S5 and S11). To generate overexpression plasmids of SlMAP70s and SlIQDs with fluorescence protein fusions, full-length sequences were firstly cloned to the V097 vector by assembly clone or T4 DNA ligase according to the primers and restriction sites (see Supplemental Table S1) and then were cloned into various destination vectors of pK7WGR2 (N-terminal RFP), pMDC43-GFP (N-terminal GFP), and pK7WGC2 (N-terminal cyan fluorescence protein [CFP]) according to the requirement via Gateway LR Clonase (Invitrogen). The primers and restriction sites used for cloning are listed in Supplemental Table S1. All the vectors used in this study were stored in our laboratory. All constructs were transformed into *Agrobacterium tumefaciens* (strain GV3101) for transformation.

Plant materials and growth conditions

Tomato (*S. lycopersicum*) cultivars MicroTom and AC were used as the WT in this study. Tomato transformation was performed as described previously (Sharma et al. 2009). Homozygous lines were used for subsequent analyses. The *Pro35S:GFP-SlMAP70-1* and *Pro35S:GFP-SlIQD21a* coexpressing plants were generated by the cross of single stable lines. The RFP-TUA5 stable transgenic plants of *N. benthamiana* were obtained from a previous study (Guo et al. 2023). The tomato seeds were germinated on 1/2 MS medium and grown on soil under a 14-h/10-h light/dark photoperiod in a growth room at 25 °C. Plants were grown under white light added with yellow light LEDs, and the light intensity was 15,000 LUX.

Fruit and ovary shape analysis

Mature tomato fruits were cut longitudinally and scanned at 600 dpi (dots per inch). Anthesis ovaries were imaged using the Leica M205 FA dissecting microscope. The maximum length and width were measured using ImageJ software, and the Fruit Shape Index (length-to-width ratio) was calculated. Three to five plants of each genotype were analyzed, and the average values were taken from at least 20 fruits or ovaries and analyzed with Tukey's test ($P < 0.05$).

Tissue fixation and sectioning

Anthesis-stage ovaries were cut longitudinally with a razor blade and fixed in PFA (4% w/v paraformaldehyde, 0.01 M PBS buffer, and pH 7.4) at 4 °C overnight. The samples were dehydrated with ethanol-ddH_2O series (50, 70, 85, 95, 100, and 100% v/v) for 1 h for each step. Then, the samples were treated with 1:1 ethanol: poly-distearate (Sigma-Aldrich) for 2 h followed by 100% poly-distearate at 38 °C for 3 h. Samples were then solidified in poly-distearate following the paraffin section's protocol. Embedded samples were cut into 12-μm sections using a Leica RM2255 automated microtome. Deparaffinization was performed with 100% ethanol for 10 min. The sections were stained with 0.01% w/v calcofluor white for 2 min, washed with water, and then imaged using a Leica TCS SP8 confocal microscope. Cell size and number were analyzed using ImageJ. The length and width of parenchyma cells in the proximal area were evaluated on at least 150 cells from 15 ovaries for each genotype analyzed with Tukey's test ($P < 0.05$). Numbers of parenchyma cells were counted in the columella area in the proximodistal and the proximal area in the mediolateral direction.

Confocal microscopy and image analysis

N. benthamiana leaves were pressure infiltrated through the abaxial epidermis with *A. tumefaciens* GV3101 cells containing the construct and the silencing suppressor p19 in a 1:1 ratio. To analyze the subcellular localization of SlMAP70 proteins during the cell division cycle, the *Pro35S:AtCYCD3;1* construct was also coinfiltrated as described (Xu et al. 2020). The images were obtained 2 d after infiltration. Images were taken with a Leica TCS SP8 inverted microscope using a 63× oil-immersion objective. The excitation wavelengths for calcofluor white/CFP, GFP, YFP, and RFP/PI were 405, 488, 514 and 552 nm, respectively, and emission was detected between 410 and 450 nm (calcofluor white), 450 and 480 nm (CFP), 505 and 550 nm (GFP), 550 and 580 nm (YFP), and 590 and 640 nm (RFP/PI). Fluorescence intensity profiles of GFP and RFP fluorescence were generated using the Plot Profile module of ImageJ. Time lapses of microtubule dynamics were acquired at 15 s/frame. Microtubule ends were artificially color-labeled using a published procedure using ImageJ (Lindeboom et al. 2013; Smertenko et al. 2020).

CMT array and cell shape analysis in tomato

To visualize the organization of CMTs in fruit cells, the ovary/fruit endocarp pavement cells from different fruit development stages were carefully dissected from the middle of the fruits (Fig. 5A). To keep the point of start consistent, the ovaries were sampled from blooming flowers that had been hand-pollinated 24 h before observation (denoted as Day 0). Then, the samples were put onto a microslide and the endocarp faced upward for observation. A cover slide was put on the samples gently, and the images were taken using confocal with settings for GFP fluorescence. For quantification of CMT arrangement in the endocarp pavement cells, the anisotropy and orientation in a whole cell were analyzed by the Fibril Tool plugin of ImageJ (Boudaoud et al. 2014). For quantification of cell shape, samples were immersed in a staining solution containing 10-μg/ml propidium iodide (Sigma-Aldrich) and incubated for at least 1 min. Leaf and endocarp pavement cells were imaged by a confocal microscope with an RFP setting, and quantified by the PaCeQuant plugin of ImageJ (Möller et al. 2017).

BiFC assays

The coding sequences (CDSs) of *SlIQD21a* and *MAP65-1* were cloned into p35S:YFPC, and CDSs of *SlMAP70-1*, *SlMAP70-2*, and *SlMAP70-3* were cloned into p35S:YFPN (Jakobson et al. 2016) vector by gateway LR reaction. Resultant constructs and control vectors were coexpressed in *N. benthamiana* leaves, and YFP fluorescence was observed by Leica TCS SP8 confocal microscope after infiltration for 3 d.

Y2H studies

Full-length *SlMAP70s* were cloned into the pGBKT7 vector, and full-length *SlIQDs* selected were cloned into the pGADT7 vector by gateway LR reaction. A pair of bait and prey constructs were cotransformed into the AH109 yeast (*Saccharomyces cerevisiae*) strain and spotted on a vector-selective medium lacking Trp and Leu (SD/-Trp/-Leu). The yeast transformants were screened on an interaction-selective medium lacking Trp, Leu, and His (SD/-Trp/-Leu/-His).

SlMAP70-1 antibody generation

DNA fragments corresponding to antigen peptide of SlMAP70-1 (amino acid residues 397 to 501) were cloned into the pET28a vector. The antigen peptide was expressed with a 6×His tag fusion on the N terminus (pET28a) in *Escherichia coli* BL21+ and then purified according to the instruction of Ni-NTA Agarose (70666-4, EMD Millipore Corporation). Purified proteins were used to raise antibodies in mice as described in (Smertenko et al. 2008). The polyclonal antibodies were tested by immunoblot in tomato plants as shown in Supplemental Fig. S4C.

Immunoblot and Co-IP assay

For immunoblot assay, samples of young leaves were collected from 1-mo-old seedlings of individual genotypes. For GFP-Trap–based Co-IP assays, GFP-SlMAP70-1 and RFP-SlIQD21a proteins were coexpressed in *N. benthamiana* leaf cells, single expression of RFP-SlIQD21a was used as a control, and the samples were collected after infiltration for 2 d. The immunoblot and Co-IP assays were performed as described previously (Li et al. 2022). The anti-GFP antibody (Biorbyt, # orb345331, 1:5,000 dilution, mouse), anti-SlMAP70-1 antibody (1:500 dilution, generated in this study), anti-RFP antibody (Abcam, #ab62341, 1:1,000 dilution, rabbit), and anti-actin (BBI, #D110007, 1:5,000 dilution, rabbit) were used as the primary antibody (25 °C, 2 h). And the goat anti-mouse (Yeasen, #33201ES60 1:10,000 dilution) and goat anti-rabbit (BBI, #D110058, 1:5,000 dilution) were used as the secondary antibody (25 °C, 1 h) according to the host species of the first antibody. For detection, the membrane was incubated in enhanced chemiluminescence (ECL) solution (36222ES60, Yeasen) and imaged using an imaging system (FluorChem M, Alpha Innotech).

Oryzalin treatment

For low-concentration oryzalin treatment for a prolonged period, seeds of different genotypes were grown on a 1/2 MS medium. After 1 wk, seedlings after germination (root length at about 1 mm) were transferred into a new medium supplement with DMSO or 300 nM oryzalin for 4 d. More than 20 individual roots were taken from every genotype. For high-concentration oryzalin treatment, stable transgenic *N. benthamiana* lines expressing *RFP-TUA5* were used (Guo et al. 2023). Leaf segments of infiltrated *N. benthamiana* expressing various microtubule-binding proteins were submerged in 100 μM oryzalin solution for different times before imaging. ImageJ software was used to quantify the numbers of CMTs in pavement cells. A fixed line (25 μm) perpendicular to the orientation of the most CMTs was drawn, and the number of CMTs across the line was counted. Two fixed-length lines were drawn for each cell, and at least 20 cells were used in each replicate. The relative CMT density of each sample (CMT relative density = density at Tn/density at T0) was calculated and analyzed with Tukey's test ($P < 0.05$) (Supplemental Data Set S1).

RNA extraction and RT-PCR analysis

The total RNA was extracted from young leaves of different tomato transgenic lines using the TRIzol Reagent (Sangon Biotech), and the first-strand cDNA was synthesized using TransScript All-in-One SuperMix (TransGen Biotech). Reverse transcription PCR (RT-PCR) was performed using 2× Taq Master Mix (Vazyme Biotech) with 1 μL of 1:10 diluted reverse transcription product in a 20-μL PCR mix. The housekeeping gene *SlActin-2*, which controlled below 25 cycles in PCR program settings, was used as a reference. The PCR products were separated by 1.5% w/v agarose gel electrophoresis and photographed for preservation. All primers used in this study are listed in Supplemental Table S2.

Gene expression heatmap and phylogenetic analysis

The transcriptome data of various tissues in tomato cultivar 'Heinz' were downloaded from the TOMATO FUNCTIONAL GENOMICS DATABASE (Tomato Genome Consortium 2012, http://ted.bti.cornell.edu/) and used for the tissue-specific analysis. MAP70 and IQD family gene expression heatmaps were analyzed using TBtool software (Chen et al. 2020). For phylogenetic analysis, multiple sequence alignment of tomato and *Arabidopsis* MAP70 proteins was conducted using MUSCLE algorithms with an open penalty of −2.9 gaps and gap extension at 0, followed by the phylogenetic tree construction using MEGA software with the maximum likelihood method and 1,000 bootstrap replicates (Kumar et al. 2016).

Accession numbers

Sequence data from this article can be found in the Solanaceae Genomics Network database under tomato gene accession numbers: *SlMAP70-1* (Solyc05g017980),

SlMAP70-2 (Solyc01g005330), *SlMAP70-3* (Solyc04g008040), *SlMAP70-4* (Solyc04g015010), *SlMAP70-5* (Solyc11g012660), *MAP65-1* (Solyc07g064970), *SlIQD1* (Solyc10g084280), *SlIQD5* (Solyc11g071840), *SlIQD12b* (Solyc04g016480), *SlIQD21a* (Solyc03g083100), *SlIQD21b* (Solyc06g052010), *SlIQD23* (Solyc 08g080470), and *SlIQD25* (Solyc12g008520).

Acknowledgments

We thank the support from microscopy core facilities of the College of Horticulture and Forestry Sciences, Huazhong Agricultural University. We thank the core facilities at the College of Life Science and Technology, Huazhong Agricultural University for the assistance with confocal. We thank Yuchen Long (National University of Singapore) and Feng Zhao (Northwestern Polytechnical University) for their advice on this work.

Author contributions

Z.B. performed the experiments and wrote the manuscript with P.W. and K.B.; Y.G. performed the Y2H-related studies; P.W. conceived and supervised the project; Y.D., J.Z., and J.Z. helped generate transgenic plants and tissue culture; X.Q. helped with confocal microscopy and participated in project progress meetings; K.B. helped with the IQD-related studies and imaging analysis; and K.B., B.O., and Y.D. proofread the manuscript and provided critical advice throughout the study.

Supplemental data

The following materials are available in the online version of this article.

Supplemental Figure S1. Hierarchical clustering of expression values of some *MAP* genes in different tissues of tomato cv. Heinz.

Supplemental Figure S2. Subcellular localization of SlMAP70 proteins during the cell division process.

Supplemental Figure S3. Characterization of *SlMAP70-1* OE and RNAi transgenic plants.

Supplemental Figure S4. Knock-down of *SlMAP70*-1 in 'AC' tomato also leads to a flatter fruit.

Supplemental Figure S5. Targeted mutagenesis of *SlMAP70* in tomato by CRISPR/Cas9 system.

Supplemental Figure S6. In nonfruit tissue, the cell morphology of *SlMAP70-1* transgenic plants was also altered.

Supplemental Figure S7. GFP-MAP65-1 labels microtubules in tomato and does not induce fruit shape alteration.

Supplemental Figure S8. Subcellular localization and expression pattern of various SUN/SlIQD proteins.

Supplemental Figure S9. SlIQD21a is likely to interact with different SlMAP70 proteins in vivo.

Supplemental Figure S10. Fruit shape study of different *SlIQDs* transgenic lines.

Supplemental Figure S11. Generated *sliqd21a* mutants in tomato by CRISPR/Cas9 system.

Supplemental Figure S12. Coexpression of *SlIQD21a* and *SlMAP70-1* further promotes tomato fruit elongation.

Supplemental Figure S13. CMT arrays labeled by GFP-MAP65-1 in endocarp cells of different genotype lines.

Supplemental Figure S14. The function of SlMAP70-1 and SlIQD21a proteins on CMT length.

Supplemental Table S1. Primers used for generating constructs.

Supplemental Table S2. Primers used for RT-PCR.

Supplemental Data Set S1. Statistical analysis.

Supplemental File S1. MAP70 sequence alignments.

Supplemental File S2. Readable tree file.

Supplemental Movie S1. *N. benthamiana* leaf pavement cells expressing microtubule marker, GFP-TUB6. GFP-TUB6-labeled microtubules were dynamic with active growth or shrinkage. This movie contains 6 frames with 15-s intervals.

Supplemental Movie S2. *N. benthamiana* leaf pavement cells expressing GFP-SlMAP70-1 and RFP-SlIQD21a. In cells coexpressing *SlMAP70-1* and *SlIQD21a*, microtubules appeared static with little growth or shrinkage. This movie contains 6 frames with 15-s intervals.

Funding

The project was supported by NSFC grants (no. 32261160371 and 92254307), the Foundation of Hubei Hongshan Laboratory (2021hszd016), and the Fundamental Research Funds for the Central Universities (2662023PY011) to P.W. and a Hubei Province Research grant (2021CFB142) to Z.B. K.B. would like to thank the Leibniz association (core funding), the DFG (grant BU2955/2-1 and BU2955/1-2) and the GIF (G-1482-423.13/2018) for financial support.

Conflict of interest statement. The authors declare that they have no conflicts of interest.

Data availability

The authors declare that all data supporting the findings of this study are available upon reasonable request.

References

Abel S, Bürstenbinder K, Müller J. The emerging function of IQD proteins as scaffolds in cellular signaling and trafficking. Plant Signal Behav. 2013:**8**(6):e24369. https://doi.org/10.4161/psb.24369

Bao Z, Xu Z, Zang J, Bürstenbinder K, Wang P. The morphological diversity of plant organs: manipulating the organization of microtubules may do the trick. Front Cell Dev Biol. 2021:**9**:649626. https://doi.org/10.3389/fcell.2021.649626

Baskin TI. Anisotropic expansion of the plant cell wall. Annu Rev Cell Dev Biol. 2005:**21**(1):203–222. https://doi.org/10.1146/annurev.cellbio.20.082503.103053

Bargel H, Neinhuis C. Tomato (*Lycopersicon esculentum* Mill.) fruit growth and ripening as related to the biomechanical properties of

fruit skin and isolated cuticle. J Exp Bot. 2005:**56**(413):1049–1060. https://doi.org/10.1093/jxb/eri098

Boudaoud A, Burian A, Borowska-Wykręt D, Uyttewaal M, Wrzalik R, Kwiatkowska D, Hamant O. Fibriltool, an ImageJ plug-in to quantify fibrillar structures in raw microscopy images. Nat Protoc. 2014:**9**(2):457–463. https://doi.org/10.1038/nprot.2014.024

Bürstenbinder K, Möller B, Plötner R, Stamm G, Hause G, Mitra D, Abel S. The IQD family of Calmodulin-binding proteins links calcium signaling to microtubules, membrane Subdomains, and the nucleus. Plant Physiol. 2017:**173**(3):1692–1708. https://doi.org/10.1104/pp.16.01743

Bürstenbinder K, Savchenko T, Müller J, Adamson AW, Stamm G, Kwong R, Zipp BJ, Dinesh DC, Abel S. *Arabidopsis* calmodulin-binding protein IQ67-domain 1 localizes to microtubules and interacts with kinesin light chain-related protein-1. J Biol Chem. 2013:**288**(3):1871–1882. https://doi.org/10.1074/jbc.M112.396200

Buschmann H, Müller S. Update on plant cytokinesis: rule and divide. Curr Opin Plant Biol. 2019:**52**:97–105. https://doi.org/10.1016/j.pbi.2019.07.003

Chen C, Chen H, Zhang Y, Thomas HR, Frank MH, He Y, Xia R. TBtools: an integrative toolkit developed for interactive analyses of big biological data. Mol Plant. 2020:**13**(8):1194–1202. https://doi.org/10.1016/j.molp.2020.06.009

Chen J, Pan B, Li Z, Xu Y, Cao X, Jia J, Shen H, Sun L. Fruit shape loci *sun*, *ovate*, *fs8.1* and their interactions affect seed size and shape in tomato. Front Plant Sci. 2023:**13**:1091639. https://doi.org/10.3389/fpls.2022.1091639

Chu YH, Jang JC, Huang Z, van der Knaap E. Tomato locule number and fruit size controlled by natural alleles of *lc* and *fas*. Plant Direct 2019:**3**(7):e00142. https://doi.org/10.1002/pld3.142

Colin L, Chevallier A, Tsugawa S, Gacon F, Godin C, Viasnoff V, Saunders TE, Hamant O. Cortical tension overrides geometrical cues to orient microtubules in confined protoplasts. Proc Natl Acad Sci U S A. 2020:**117**(51):32731–32738. https://doi.org/10.1073/pnas.2008895117

Dou J, Zhao S, Lu X, He N, Zhang L, Ali A, Kuang H, Liu W. Genetic mapping reveals a candidate gene (*ClFS1*) for fruit shape in watermelon (*Citrullus lanatus* L). Theor Appl Genet. 2018:**131**(4):947–958. https://doi.org/10.1007/s00122-018-3050-5

Duan P, Xu J, Zeng D, Zhang B, Geng M, Zhang G, Huang K, Huang L, Xu R, Ge S, et al. Natural variation in the promoter of *GSE5* contributes to grain size diversity in rice. Mol Plant. 2017:**10**(5):685–694. https://doi.org/10.1016/j.molp.2017.03.009

Eng RC, Sampathkumar A. Getting into shape: the mechanics behind plant morphogenesis. Curr Opin Plant Biol. 2018:**46**:25–31. https://doi.org/10.1016/j.pbi.2018.07.002

Guo Y, Bao Z, Deng Y, Li Y, Wang P. Protein subcellular localization and functional studies in horticultural research: problems, solutions, and new approaches. Hortic Res. 2023:**10**(2):uhac271. https://doi.org/10.1093/hr/uhac271

Huang Z, Van Houten J, Gonzalez G, Xiao H, van der Knaap E. Genome-wide identification, phylogeny and expression analysis of *SUN*, *OFP* and *YABBY* gene family in tomato. Mol Genet Genomics. 2013:**288**(3-4):111–129. https://doi.org/10.1007/s00438-013-0733-0

Jakobson L, Vaahtera L, Tõldsepp K, Nuhkat M, Wang C, Wang YS, Hõrak H, Valk E, Pechter P, Sindarovska Y, et al. Natural variation in *Arabidopsis* cvi-0 accession reveals an important role of MPK12 in guard cell CO_2 signaling. PLoS Biol. 2016:**14**(12):e2000322. https://doi.org/10.1371/journal.pbio.2000322

Jiang L, Yan S, Yang W, Li Y, Xia M, Chen Z, Wang Q, Yan L, Song X, Liu R, et al. Transcriptomic analysis reveals the roles of microtubule-related genes and transcription factors in fruit length regulation in cucumber (*Cucumis sativus* L). Sci Rep. 2015:**5**(1):8031. https://doi.org/10.1038/srep08031

Kirik V, Herrmann U, Parupalli C, Sedbrook JC, Ehrhardt DW, Hülskamp M. CLASP localizes in two discrete patterns on cortical microtubules and is required for cell morphogenesis and cell division in *Arabidopsis*. J Cell Sci. 2007:**120**(Pt 24):4416–4425. https://doi.org/10.1242/jcs.024950

Korolev AV, Buschmann H, Doonan JH, Lloyd CW. AtMAP70-5, a divergent member of the MAP70 family of microtubule-associated proteins, is required for anisotropic cell growth in *Arabidopsis*. J Cell Sci. 2007:**120**(Pt 13):2241–2247. https://doi.org/10.1242/jcs.007393

Korolev AV, Chan J, Naldrett MJ, Doonan JH, Lloyd CW. Identification of a novel family of 70 kDa microtubule-associated proteins in *Arabidopsis* cells. Plant J. 2005:**42**(4):547–555. https://doi.org/10.1111/j.1365-313X.2005.02393.x

Kumar S, Stecher G, Tamura K. MEGA7: molecular evolutionary genetics analysis version 7.0 for bigger datasets. Mol Biol Evol. 2016:**33**(7):1870–1874. https://doi.org/10.1093/molbev/msw054

Kumari P, Dahiya P, Livanos P, Zergiebel L, Kölling M, Poeschl Y, Stamm G, Hermann A, Abel S, Müller S, et al. IQ67 DOMAIN proteins facilitate preprophase band formation and division-plane orientation. Nat Plants. 2021:**7**(6):739–747. https://doi.org/10.1038/s41477-021-00923-z

Li C, Duckney P, Zhang T, Fu Y, Li X, Kroon J, De Jaeger G, Cheng Y, Hussey PJ, Wang P. Trab family proteins are components of ER-mitochondrial contact sites and regulate ER-mitochondrial interactions and mitophagy. Nat Commun. 2022:**13**(1):5658. https://doi.org/10.1038/s41467-022-33402-w

Li Y, Deng M, Liu H, Li Y, Chen Y, Jia M, Xue H, Shao J, Zhao J, Qi Y, et al. ABNORMAL SHOOT 6 interacts with KATANIN 1 and SHADE AVOIDANCE 4 to promote cortical microtubule severing and ordering in *Arabidopsis*. J Integr Plant Biol. 2021:**63**(4):646–661. https://doi.org/10.1111/jipb.13003

Lindeboom JJ, Nakamura M, Hibbel A, Shundyak K, Gutierrez R, Ketelaar T, Emons AM, Mulder BM, Kirik V, Ehrhardt DW. A mechanism for reorientation of cortical microtubule arrays driven by microtubule severing. Science 2013:**342**(6163):1245533. https://doi.org/10.1126/science.1245533

Liu J, Chen J, Zheng X, Wu F, Lin Q, Heng Y, Tian P, Cheng Z, Yu X, Zhou K, et al. *GW5* Acts in the brassinosteroid signalling pathway to regulate grain width and weight in rice. Nat Plants. 2017:**3**(5):17043. https://doi.org/10.1038/nplants.2017.43

Liu J, Van Eck J, Cong B, Tanksley SD. A new class of regulatory genes underlying the cause of pear-shaped tomato fruit. Proc Natl Acad Sci U S A. 2002:**99**(20):13302–13306. https://doi.org/10.1073/pnas.162485999

Liu Z, Schneider R, Kesten C, Zhang Y, Somssich M, Zhang Y, Fernie AR, Persson S. Cellulose-microtubule uncoupling proteins prevent lateral displacement of microtubules during cellulose synthesis in *Arabidopsis*. Dev Cell. 2016:**38**(3):305–315. https://doi.org/10.1016/j.devcel.2016.06.032

Mitra D, Klemm S, Kumari P, Quegwer J, Möller B, Poeschl Y, Pflug P, Stamm G, Abel S, Bürstenbinder K. Microtubule-associated protein IQ67 DOMAIN5 regulates morphogenesis of leaf pavement cells in *Arabidopsis thaliana*. J Exp Bot. 2019:**70**(2):529–543. https://doi.org/10.1093/jxb/ery395

Möller B, Poeschl Y, Plötner R, Bürstenbinder K. Pacequant: a tool for high-throughput quantification of pavement cell shape characteristics. Plant Physiol. 2017:**175**(3):998–1017. https://doi.org/10.1104/pp.17.00961

Montesinos JC, Abuzeineh A, Kopf A, Juanes-Garcia A, Ötvös K, Petrášek J, Sixt M, Benková E. Phytohormone cytokinin guides microtubule dynamics during cell progression from proliferative to differentiated stage. EMBO J. 2020:**39**(17):e104238. https://doi.org/10.15252/embj.2019104238

Morejohn LC, Bureau TE, Molè-Bajer J, Bajer AS, Fosket DE. Oryzalin, a dinitroaniline herbicide, binds to plant tubulin and inhibits microtubule polymerization in vitro. Planta 1987:**172**(2):252–264. https://doi.org/10.1007/bf00394595

Muños S, Ranc N, Botton E, Bérard A, Rolland S, Duffé P, Carretero Y, Le Paslier MC, Delalande C, Bouzayen M, et al. Increase in tomato locule number is controlled by two single-nucleotide polymorphisms located near WUSCHEL. Plant Physiol. 2011:**156**(4): 2244–2254. https://doi.org/10.1104/pp.111.173997

Pan Y, Liang X, Gao M, Liu H, Meng H, Weng Y, Cheng Z. Round fruit shape in WI7239 cucumber is controlled by two interacting quantitative trait loci with one putatively encoding a tomato *SUN* homolog. Theor Appl Genet. 2017:**130**(3):573–586. https://doi.org/10.1007/s00122-016-2836-6

Pan Y, Wang Y, McGregor C, Liu S, Luan F, Gao M, Weng Y. Genetic architecture of fruit size and shape variation in cucurbits: a comparative perspective. Theor Appl Genet. 2020:**133**(1):1–21. https://doi.org/10.1007/s00122-019-03481-3

Pesquet E, Korolev AV, Calder G, Lloyd CW. Mechanisms for shaping, orienting, positioning and patterning plant secondary cell walls. Plant Signal Behav. 2011:**6**(6):843–849. https://doi.org/10.4161/psb.6.6.15202

Ren H, Dang X, Cai X, Yu P, Li Y, Zhang S, Liu M, Chen B, Lin D. Spatio-temporal orientation of microtubules controls conical cell shape in *Arabidopsis thaliana* petals. PLoS Genet. 2017:**13**(6): e1006851. https://doi.org/10.1371/journal.pgen.1006851

Riglet L, Rozier F, Kodera C, Bovio S, Sechet J, Fobis-Loisy I, Gaude T. KATANIN-dependent mechanical properties of the stigmatic cell wall mediate the pollen tube path in *Arabidopsis*. eLife. 2020:**9**: e57282. https://doi.org/10.7554/eLife.57282

Robinson S, Kuhlemeier C. Global compression reorients cortical microtubules in *Arabidopsis* hypocotyl epidermis and promotes growth. Curr Biol. 2018:**28**(11):1794–1802.e2. https://doi.org/10.1016/j.cub.2018.04.028

Schaefer E, Belcram K, Uyttewaal M, Duroc Y, Goussot M, Legland D, Laruelle E, de Tauzia-Moreau ML, Pastuglia M, Bouchez D. The preprophase band of microtubules controls the robustness of division orientation in plants. Science 2017:**356**(6334):186–189. https://doi.org/10.1126/science.aal3016

Sharma MK, Solanke AU, Jani D, Singh Y, Sharma AK. A simple and efficient *Agrobacterium*-mediated procedure for transformation of tomato. J Biosci. 2009:**34**(3):423–433. https://doi.org/10.1007/s12038-009-0049-8

Smertenko AP, Kaloriti D, Chang H, Fiserova J, Opatrny Z, Hussey PJ. The C-Terminal variable region specifies the dynamic properties of Arabidopsis microtubule-associated protein MAP65 isotypes. Plant Cell. 2008:**20**(12):3346–3358. http://dx.doi.org/10.1105/tpc.108.063362

Smertenko T, Turner G, Fahy D, Brew-Appiah RAT, Alfaro-Aco R, de Almeida Engler J, Sanguinet KA, Smertenko A. *Brachypodium distachyon* MAP20 functions in metaxylem pit development and contributes to drought recovery. New Phytol. 2020:**227**(6):1681–1695. http://dx.doi.org/10.1111/nph.16383

Spinner L, Gadeyne A, Belcram K, Goussot M, Moison M, Duroc Y, Eeckhout D, De Winne N, Schaefer E, Van De Slijke E, et al. A protein phosphatase 2A complex spatially controls plant cell division. Nat Commun. 2013:**4**(1):1863. https://doi.org/10.1038/ncomms2831

Stöckle D, Reyes-Hernández BJ, Barro AV, Nenadić M, Winter Z, Marc-Martin S, Bald L, Ursache R, Fujita S, Maizel A, et al. Microtubule-based perception of mechanical conflicts controls plant organ morphogenesis. Sci Adv. 2022:**8**(6):eabm4974. https://doi.org/10.1126/sciadv.abm4974

Sumino Y, Nagai KH, Shitaka Y, Tanaka D, Yoshikawa K, Chaté H, Oiwa K. Large-scale vortex lattice emerging from collectively moving microtubules. Nature 2012:**483**(7390):448–452. https://doi.org/10.1038/nature10874

Thompson DS, Davies WJ, Ho LC. Regulation of tomato fruit growth by epidermal cell wall enzymes. Plant Cell Environ. 1998:**21**(6): 589–599. https://doi.org/10.1046/j.1365-3040.1998.00308.x

Tomato Genome Consortium. The tomato genome sequence provides insights into fleshy fruit evolution. Nature 2012:**485**(7400):635–641. https://doi.org/10.1038/nature11119

Wang X, Ma Q, Wang R, Wang P, Liu Y, Mao T. Submergence stress-induced hypocotyl elongation through ethylene signaling-mediated regulation of cortical microtubules in *Arabidopsis*. J Exp Bot. 2020:**71**(3):1067–1077. https://doi.org/10.1093/jxb/erz453

Wu S, Xiao H, Cabrera A, Meulia T, van der Knaap E. *SUN* regulates vegetative and reproductive organ shape by changing cell division patterns. Plant Physiol. 2011:**157**(3):1175–1186. https://doi.org/10.1104/pp.111.181065

Wu S, Zhang B, Keyhaninejad N, Rodríguez GR, Kim HJ, Chakrabarti M, Illa-Berenguer E, Taitano NK, Gonzalo MJ, Díaz A, et al. A common genetic mechanism underlies morphological diversity in fruits and other plant organs. Nat Commun. 2018:**9**(1):4734. https://doi.org/10.1038/s41467-018-07216-8

Xiao H, Jiang N, Schaffner E, Stockinger EJ, van der Knaap E. A retrotransposon-mediated gene duplication underlies morphological variation of tomato fruit. Science 2008:**319**(5869):1527–1530. https://doi.org/10.1126/science.1153040

Xu J, Lee YJ, Liu B. Establishment of a mitotic model system by transient expression of the D-type cyclin in differentiated leaf cells of tobacco (*Nicotiana benthamiana*). New Phytol. 2020:**226**(4): 1213–1220. https://doi.org/10.1111/nph.16309

Yang B, Wendrich JR, De Rybel B, Weijers D, Xue HW. Rice microtubule-associated protein IQ67-DOMAIN14 regulates grain shape by modulating microtubule cytoskeleton dynamics. Plant Biotechnol J. 2020:**18**(5):1141–1152. https://doi.org/10.1111/pbi.13279

Zang J, Klemm S, Pain C, Duckney P, Bao Z, Stamm G, Kriechbaumer V, Bürstenbinder K, Hussey PJ, Wang P. A novel plant actin-microtubule bridging complex regulates cytoskeletal and ER structure at ER-PM contact sites. Curr Biol. 2021:**31**(6):1251–1260.e4. https://doi.org/10.1016/j.cub.2020.12.009

Zhao F, Du F, Oliveri H, Zhou L, Ali O, Chen W, Feng S, Wang Q, Lü S, Long M, et al. Microtubule-mediated wall anisotropy contributes to leaf blade flattening. Curr Biol. 2020:**30**(20):3972–3985.e6. https://doi.org/10.1016/j.cub.2020.07.076

Zhou H, Ma R, Gao L, Zhang J, Zhang A, Zhang X, Ren F, Zhang W, Liao L, Yang Q, et al. A 1.7-Mb chromosomal inversion downstream of a *PpOFP1* gene is responsible for flat fruit shape in peach. Plant Biotechnol J. 2021:**19**(1):192–205. https://doi.org/10.1111/pbi.13455